



DEPARTMENT OF ELECTRONIC AND
TELECOMMUNICATION ENGINEERING

UNIVERSITY OF MORATUWA
SRI LANKA

An AI-Powered Wireless EEG Amplifier
for Detecting Neonatal Seizures

FINAL PROJECT REPORT
SUBMITTED IN PARTIAL FULFILLMENT OF THE REQUIREMENTS FOR THE COURSE
MODULE BM4200
JUNE 26, 2024

SUPERVISORS:

Dr. Chamira Edussooriya
Dr. Anjula De Silva
Prof. Jithangi Wanigasinghe

MEMBERS:

Akila Abeyratne	190009U
Dinuka Sandun	190639B
Kavindu Weerasinghe	190672T
Nima Wickramasinghe	190688X

GROUP 13

Approval of the Department of Electronic & Telecommunication Engineering

.....

Head, Department of Electronic &
Telecommunication Engineering

This is to certify that I/we have read this project and that in my/our opinion it is fully adequate, in scope and quality, as an Undergraduate Graduation Project.

Supervisor: Dr. Chamira Edussooriya

Signature:

Date:

Supervisor: Dr. Anjula De Silva

Signature:

Date:

Declaration

This declaration is made on June 26, 2024.

We declare that the dissertation titled AI Powered Wireless Neonatal Seizure Detection Device and the work presented in it are our own. We confirm that:

- this work was done wholly or mainly in candidature for a B.Sc. Engineering degree at this university,
- where any part of this dissertation has previously been submitted for a degree or any other qualification at this university or any other institute has been clearly stated,
- where we have consulted the published work of others, is always clearly attributed,
- where we have quoted from the work of others, the source is always given.
- with the exception of such quotations, this dissertation is entirely our own work,
- we have acknowledged all main sources of help,
- parts of this dissertation have been published.

.....
DATE

.....
AKILA ABEYRATNE
(190009U)

.....
DINUKA SANDUN
(190639B)

.....
KAVINDU WEERASINGHE
(190672T)

.....
NIMA WICKRAMASINGHE
(190688X)

Preface

This report was composed as a partial fulfilment of the requirements of Module EN4202 - Project, in the curriculum of B.Sc. in Engineering (Electronic and Telecommunication) at the University of Moratuwa, Sri Lanka. The experience and knowledge that we gained during the final year project were used and were the inspiration to create this report.

Abstract

Seizures can occur at any age due to abnormal brain electrical activity. Detecting seizures in neonates is crucial. Neonatal seizures can be hard to spot as they may seem like normal behaviour. Early diagnosis and treatment are vital to prevent brain damage and long-term complications. Continuous EEG monitoring with wet electrodes, interpreted by an experienced neurologist, is the current gold standard for detecting neonatal seizures. However, this system is expensive and not widely accessible.

Objectives: In this work, a low-cost wireless EEG headset with dry-active electrodes is proposed, thereby reducing the tedious process associated with neonatal EEG preparation. Alongside hardware designs, a novel deep learning model is being introduced for real-time seizure detection, along with an artifact removal algorithm and a Graphical User Interface that encompasses all these components.

Methodology: This headset system comprises eight dry active electrodes for signal conditioning, a low noise analog front end with an ADS1299 Integrated Circuit (IC) and an integrated Inertial Measurement Unit (IMU) sensor, and a wireless microcontroller unit, all in a small form factor. The acquired EEG signal from this headset is transmitted to a computer for further processing. The processed signal is input to the deep learning model to detect seizures where temporal features are extracted by a convolutional encoder and spatial features are extracted by a graph attention network. Also, this model explains the binary class output (seizure or non-seizure) by the Grad-CAM architecture. The signal is processed and analyzed to remove artifacts using independent component analysis to extract temporal, spatial, and spectral information. A noise component labelling model detects and removes artifacts, resulting in a clean signal.

Results: The system was tested on an absence seizure patient at Lady Ridgeway Hospital (LRH). The quality of the signals obtained from our dry electrode system exhibits a higher signal-to-noise ratio than the commercial gold standard wet-electrode EEG acquisition system available at LRH and was able to detect seizures in real-time. Furthermore, the proposed deep learning model demonstrates significant improvements in automatic seizure detection. An absolute improvement of 8.31% and 42.86% is observed in AUC and recall for the Zenodo dataset under 10-fold cross-validation. The artifact removal algorithm was trained using the EPIC dataset, which contains data on patients with epileptic seizures. Therefore, it could differentiate between artifacts and seizures on the data acquired at LRH compared to the preexisting ICA label model available in the main library.

Acknowledgment

In the course of our final year project, we are indebted to numerous individuals whose invaluable support and guidance made this endeavour possible. We extend our heartfelt thanks to Dr. Ranga Rodrigo, the outgoing head of the department, Dr. Subramaniam Thayaparan the newly appointed head of the department along with all the lecturers and officials who worked tirelessly in identifying and providing us with promising project opportunities for our final year. A special thanks go to Dr. Mevan Gunawardena, our project coordinator, for the consistent guidance and support given throughout this project.

Our heartfelt gratitude goes to our principal supervisor, Dr. Chamira Edussooriya, whose support, mentorship, and encouragement helped us overcome challenges and progress with our project till the end making it a huge success. We especially thank Prof. Jithangi Wanigasinghe professor in paediatric neurology at the Department of Paediatrics, Faculty of Medicine, University of Colombo for constant support and feedback given from the medical aspect of the project along with the staff of the Lady Ridgeway Hospital for Children for allowing and supporting us to do a clinical trial of our device. We are also grateful to Dr. Anjula De Silva for the advice given throughout the project as a co-supervisor. A special gratitude goes to our external supervisor Mr. Kithmin Wickramasinghe for the guidance given throughout the project with valuable feedback on every aspect and for helping us draft the research paper.

The computational resources used in the project were funded by the Accelerating Higher Education Expansion and Development (AHEAD) Operation of the Ministry of Higher Education of Sri Lanka funded by the World Bank. We thank Dr. Ranga Rodrigo for granting us access to the Baker server.

Another aspect we are thankful for is the insightful evaluations provided by the panel of lecturers. Their constructive feedback and valuable suggestions during the feasibility presentation, mid-progress presentations, final demonstration, and final presentation significantly contributed to the improvement of our project's outcomes. Their valuable input helped us refine our approach and achieve more comprehensive results.

We also extend our sincere appreciation to the non-academic staff at the Department of Electronic and Telecommunication Engineering for the support given at laboratories to conduct the necessary device laboratory testing

It is with immense gratitude that we acknowledge the support and assistance of all these individuals. Their contributions played a pivotal role in the successful completion of our final-year project, and we are truly thankful for their encouragement, guidance, and mentorship.

Contents

1	Introduction	14
1.1	Problem Statement	14
1.2	Related Work	14
1.3	Objectives and Scope	15
2	Literature Review	16
2.1	Headset Design	16
2.2	Electrode Design	17
2.3	Analog Front End	19
2.4	Microcontroller Unit	20
2.5	Machine Learning	20
2.6	Signal Processing	21
3	Methodology	23
3.1	Overview	23
3.2	Hardware	24
3.2.1	Headset Design	25
3.2.2	Electrode Design	26
3.2.3	Analog Front End	28
3.2.4	Microcontroller Unit	31
3.2.5	Total Cost of Product	33
3.3	Software	33
3.3.1	Machine Learning	34
3.3.2	Signal Processing	41
3.3.3	Graphical User Interface	46
3.4	Clinical Trials	49
4	Results and Discussion	50
4.1	Signal Quality	50
4.2	Specifications of the Device	52
4.3	Machine Learning	53
4.4	Signal Processing	55
4.5	Device User Feedback	59

5 Conclusion	61
References	61
Appendices	67
A PCB and Schematics	68
B Information Sheet	81

List of Figures

2.1	Comparison between 10-20 system and reduced electrode system for EEG signal acquisition [1]	16
2.2	Ag/AgCl multi-spike electrodes	18
2.3	Different shielding methods	19
2.4	Usual elements of an AFE	19
3.1	Overall block diagram	23
3.2	Hardware block diagram	24
3.3	Different headset designs tried throughout the project	25
3.4	Final EEG headset design	26
3.5	Designed active electrode used for EEG signal acquisition	27
3.6	Analog front end	28
3.7	Breadboard design	28
3.8	Results from the breadboard design	29
3.9	Dotboard design	29
3.10	Results from the dotboard design	30
3.11	Microcontroller unit	31
3.12	Microcontroller unit design	32
3.13	Software block diagram	34
3.14	(a) The illustration of employed reduced electrode montage Graph representation of the selected electrode montage. (b) Node represents the channels and edges represent the functional connectivity between channels.	34
3.15	Full deep learning model	36
3.16	The first 4 blocks belong to the CNN-based temporal feature extractor. The 12 channels are preserved throughout the CNN encoder but down-sampled the temporal features at the end of each block using Average Pooling.	37
3.17	GAT layers 1, 2, and 3 have the output shapes (12×37) , (12×32) , and (12×16) respectively and the last MLP network has 32, 16, and 1 neurons respectively.	38
3.18	Performance comparison between GAT layers and scaled dot product attention layers. Training for dot product attention was terminated after 50 epochs as it has low performance	39
3.19	Signal processing pipeline	42
3.20	Independent component label model architecture	45
3.21	Expected flow when using the GUI	46

3.22	Check connectivity interface with O1 channel not in contact	47
3.23	IMU data interface with movement detection	47
3.24	Live run while data are recorded	48
3.25	Clinical testing on an absence seizure patient with both the commercial wet electrode system and our dry electrode system	49
4.1	EEG during eyes open	50
4.2	EEG during eyes closed	50
4.3	EEG during seizure	51
4.4	Correlation between data recorded from wet electrode and dry electrode system	52
4.5	FFT of recorded data during various states	52
4.6	SNR of recorded data	53
4.7	Visualization of the epoch with its heatmap. Dark blue represents the zero relevance while dark red represents the highest relevance. The relevance is given as probability. This is a seizure epoch and the model detected this as a seizure epoch.	54
4.8	Independent component classified as artifact	56
4.9	Independent component classified as brain waves from a seizure onset	56
4.10	Independent component removing eye artifacts from the data obtained at Lady Ridgeway Hospital	57
4.11	Independent component retaining seizures from the data obtained at Lady Ridgeway Hospital	57
4.12	Independent component failing to remove eye artifacts from the data obtained at Lady Ridgeway Hospital - using mne ICAlabeling method	58
4.13	Independent component retaining seizures from the data obtained at Lady Ridgeway Hospital - using mne ICAlabeling method	58
4.14	Independent component removing eye artifacts from the data obtained at Lady Ridgeway Hospital - using ATAR method	58
4.15	Independent component removing seizures from the data obtained at Lady Ridgeway Hospital - using ATAR method	58
4.16	Improvement of time compared to the conventional device	59
4.17	Amount of comfortability while wearing the device	60
4.18	Amount of comfortability after removing the device	60
4.19	Electrode mark visibility with time	60
A.1	AFE - 3D view - bottom	68
A.2	AFE - 3D view - top	69
A.3	AFE top layer	69
A.4	AFE bottom layer	70
A.5	AFE power layer	70
A.6	AFE ground layer	71
A.7	MCU - 3D view - bottom	71
A.8	MCU - 3D view - top	72
A.9	MCU top layer	72
A.10	MCU bottom layer	73

A.11 MCU power layer	73
A.12 MCU ground layer	74
A.13 ADS1299 circuitry	75
A.14 Power for ADS1299	76
A.15 5V supply for ADS1299	76
A.16 ESP32 circuitry	76
A.17 3.3V supply for ESP32	77
A.18 Battery charging circuit	77
A.19 IMU circuitry	78
A.20 USB isolator	78
A.21 Active electrode - 3D view - top	78
A.22 Active electrode - 3D view - bottom	79
A.23 Active electrode top layer	79
A.24 Active electrode bottom layer	79
A.25 Active electrode schematics	80

List of Tables

2.1	Electrode classification according to connectivity medium	17
3.1	Different status indicated by the LEDs	32
3.2	Cost breakdown for the product	33
3.3	Model structure. N- Number of filters, K- kernel shape, W- Transformation matrix, a- shared attention vector. All Convolution layers use zero padding and stride 1	40
4.1	Dataset used to calculate signal quality	51
4.2	Device specifications	53
4.3	Model performance comparison. CV- Cross Validation	55
4.4	Model performance comparison of the IC label model	55

Abbreviations

ADC Analog to Digital Converter

AFE Analog Front End

AI Artificial Intelligence

BSS Blind Source Separation

CNN Convolutional Neural Network

DNN Deep Neural Network

DRL Driven Right Leg

EEG Electroencephalogram

ESD Electro-Static Discharge

IC Integrated Circuit

ICA Independant Componenet Analysis

IMU Inertial Measurement Unit

LIME Local Interpretable Model Agnostic Explanations

PDF Probability Density Function

PSD Power Spectral Density

seCAM Segmentation Class Activation Mapping

SNR Signal to Noise Ratio

SVM Support Vector Machine

Chapter 1

Introduction

1.1 Problem Statement

Seizures can happen to anyone, regardless of their age, and are caused by abnormal electrical activity in the brain. Detecting seizures in newborns, particularly during the first four weeks after birth (known as the neonatal period), is a crucial task. Neonatal seizures can be challenging to identify as they are often subtle and can be mistaken for normal behaviour. On the other hand, seizures in adults are easier to recognize, as they exhibit noticeable physical symptoms. It is essential to diagnose and treat neonatal seizures early to prevent any harm to the baby's developing brain and avoid any long-lasting complications. Therefore, the necessity of well-experienced neurologists is a must to identify neonatal seizures.

The incidences of neonatal seizures vary widely based on the geographical location, the definition of neonatal seizures, and the technology used for seizure detection. According to the quantitative analysis records, there are 95 cases per 1000 live births of preterm infants and 3 cases per 1000 live births of normal infants [2]. With the lack of experienced neurologists and technology to identify neonatal seizures, some countries show a large incident rate. For example, since there are fewer facilities in Sri Lankan neonatal intensive care units (NICU) these numbers can be higher [3].

1.2 Related Work

EEG is a non-invasive medical technique that measures electrical activity generated by the brain. This electrical activity, recorded from the scalp using electrodes, reflects the synchronized firing of large populations of neurons [4]. In the hospital setups, they use the gold standard method to acquire Electroencephalogram (EEG) from patients. They use wet electrodes to get the scalp EEG. In this case, conductive gel is applied to create a proper conductive medium between electrodes and the scalp. Even after acquiring EEG data, a well-trained neurologist is needed to identify seizures. Apart from these signals, they monitor the neonate through a video feed for the whole time they obtain eeg from the neonate [5].

Chen. H *et al.* [6] created a system to detect seizures in babies using other measurements like heart rate, breathing, and movement. This system skips the brain activity recording (EEG) altogether. Because it doesn't use EEG, this method isn't ideal. Another team led by Shih-Kai *et al.* [7] designed a headband to detect seizures with EEG, but it has limitations. The headband uses fabric sensors that can't reach the scalp through hair, and it doesn't cover the entire head, leading to inaccurate results.

The gold standard method of transmitting EEG signals to the computer involves using wires, which can be messy. To address this issue, Omurtag et al [8]. developed a wireless EEG device, but it was not specifically designed for seizure detection and used wet electrodes to acquire signals. On the other hand, Grummert et al. [9] developed a dry electrode-based wireless EEG system that can detect seizures, but is less adjustable than the wet electrode system and doesn't produce as accurate results. Additionally, it is quite expensive.

1.3 Objectives and Scope

The main objective of this project is to design an AI-powered user-friendly neonatal seizure detection device. Under this primary objective, we carry out the following studies to mitigate the system issues stated in section 1.2.

1. Low noise dry electrode-based EEG acquisition
2. User-friendly and highly adjustable headset design
3. Seizure detection
4. Interpretability
5. Artifact removal

Chapter 2

Literature Review

2.1 Headset Design

Capturing of EEG signals of neonates can be done in both the international 10-20 system and the reduced electrode montage, which only uses 8 electrodes and reference. A study was done by [1] to compare the 10-20 system with the reduced electrode montage to figure out the ability to detect and characterize neonatal seizures. It was found that the sensitivity and specificity to detect seizures using the reduced montage were 96.8% and 100%, respectively [1].

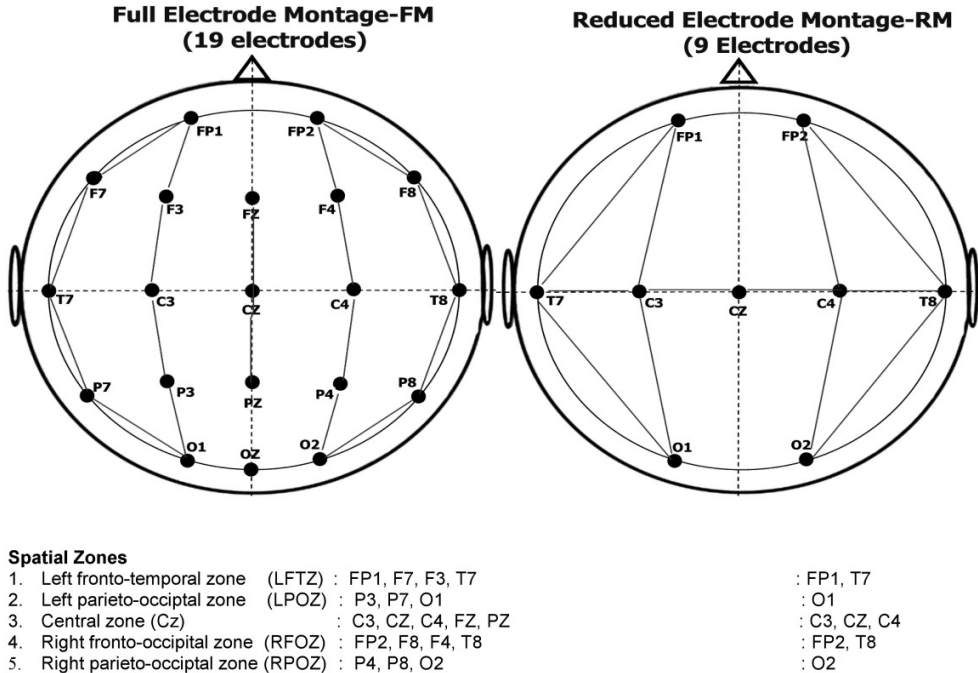


Figure 2.1: Comparison between 10-20 system and reduced electrode system for EEG signal acquisition [1]

2.2 Electrode Design

Electrodes used for EEG signal acquisition can be divided into several groups based on different criteria.

1. Connectivity Medium [10]
2. Shape [11]
3. Material Used [12]

Table 2.1: Electrode classification according to connectivity medium

Electrode Type	Pros	Cons
Wet	Golden standard High-density EEG recordings Very high signal quality Less susceptible to main interference	Skin preparation required Preparation time can be long Inconvenient for participants Conductive gel drying out
Semi-Dry	Quicker setup time than gel electrodes Quicker clean-up than gel electrodes Lower impedance than in dry electrodes	Dry quicker compared to gel electrodes More susceptible to mains interference Contact quality less due to hair
Dry	Quicker setup time than gel electrodes Skin preparation not required Suitable for at-home testing Can cooperate with hair	Difficulty keeping electrodes fixed High signal instability and higher impedance More susceptible to mains interference

According to [11] shapes of electrodes can be mainly classified into 3 categories,

1. Corn-shaped
2. Multi Spikes
3. Flat

The corn-shaped electrode causes the most discomfort and the flat electrodes are not able to penetrate the hair layer. The multi-spike-shaped electrodes overcome these 2 problems.

The research conducted by [12] compares the following different materials for the electrodes.

1. Ag Electrode
2. Ag/AgCl Electrode
3. Gold Electrode
4. Stainless-Steel AISI304

It mentions that after the study is done in a well-controlled analysis, which has also considered different motion artifacts, line noise and junction potentials, the Ag/AgCl Electrodes performed the best. Also, it says that the Ag/AgCl electrodes are three times better compared to the stainless-steel electrodes.[12]

Using active electrodes is another method to capture EEG signals A buffer amplifier on the electrode is used to reduce mains interference and wire movement artifacts. The main drawback of active electrodes is that they increase the electrode size and weight. Passive



Figure 2.2: Ag/AgCl multi-spike electrodes

electrodes connecting the cable to a high-impedance amplifier are susceptible to electrical mains interference due to their length and impedance. The buffer amplifier connects the cable to a low-output impedance buffer, minimizing interference voltage. This also shortens the high-impedance node between the amplifier and electrode.[13].

A study investigated the performance of conventional and active dry electrodes in EEG recordings. While electrode placement variations caused minor signal discrepancies, dry electrodes showed slightly higher offset, baseline drift, and low-frequency noise power. However, it had a lower power line interference at 50Hz compared to conventional wet electrodes, which is a potential advantage for specific EEG applications. An OPA2376 op amp is used at the active electrode to achieve this performance.[14]

Once the EEG signals are captured from the electrodes, they need to be sent to the PCB where data transmission/signal processing is happening. Cables are required for this transmission of data. When the data is transmitted through cables, different interferences can occur. To reduce these external interferences on the wires, shielding can be done. Wire shielding can be done mainly in three ways[15].

1. Ground Shield
2. Bias Shield
3. Active Shield

The diagram below shows how the above three shielding mechanisms look like.

Unshielded cables expose signals to interference, causing issues for low-amplitude, high-impedance EEG signals. Ground shielding, while better, still allows distributed resistance and capacitance between the shield and core. Bias shielding actively drives the shield, mitigating interference effects, and nullifying resistance and capacitance between shield and core. Active shielding connects the shield to a low-resistance source, ensuring minimal interference and signal integrity. Among these approaches, active shielding is the most effective choice for preserving the quality of biopotential signals during transmission.[15]

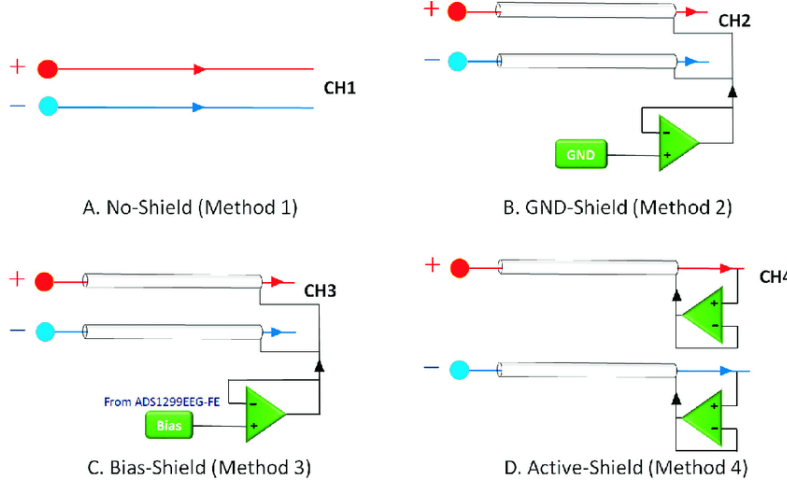


Figure 2.3: Different shielding methods

2.3 Analog Front End

To process EEG signals, it is necessary to convert them to digital form. Due to their low amplitude, vulnerability to noise, and weak nature, EEGs require an Analog Front End (AFE) before digitization.

An AFE acts as an important intermediary stage, preparing the EEG signal for accurate digital conversion. It typically comprises several key elements fig. 2.4.

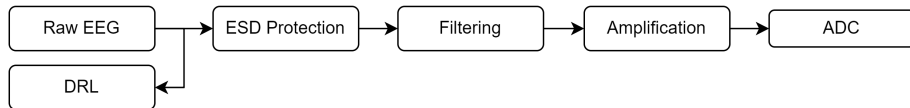


Figure 2.4: Usual elements of an AFE

The Driven Right Leg (DRL) circuit is commonly used in biosignal acquisition circuits to reduce common mode noise [16].

Previous work done in EEG signal acquisition usually contains an initial analog preprocessing stage. These contain components for Electro-Static Discharge (ESD) safety and bandpass filtering to isolate the relevant EEG frequency components [17, 18].

To amplify the weak EEG signals while minimizing noise, instrumentation amplifiers are frequently employed [19]. However, with a growing number of EEG channels, the component count increases proportionally, posing design challenges.

The ADS1299 IC by Texas Instruments is a popular choice for EEG acquisition systems due to its advantageous features: low noise operation, an 8-channel 24-bit Analog to Digital Converter (ADC), built-in DRL circuit, and high input impedance. Studies have demonstrated the effectiveness of the ADS1299 in achieving high-quality EEG signal acquisition

[17, 20, 18]. A review on using ADS1299 IC for EEG signal acquisition shows its performance capabilities for high-quality EEG signal acquisition [21].

AEFs play a vital role in ensuring the integrity and accuracy of EEG signals before digital conversion. By understanding the components and considerations involved in AFE design, researchers can optimize EEG acquisition systems for various applications.

2.4 Microcontroller Unit

An FDA-approved wireless device *microEEG[®]* is used in [22] at a Neonatal Intensive Care Unit (NICU) for EEG signal transmission. But, the device is kept away from the neonate's head and not above it. It uses Bluetooth[®] technology for data transmission.[22]

ANNE[®] One by Sibel Health is an ICU-grade wearable sensor which is used in [23] and it is used to wireless monitor neonatal vital signs. This device uses Bluetooth[®] technology for data transmission [24] and is placed on the chest. However, it does not capture any EEG signals.

There is no literature or product in the market with FDA approval where a wireless module for data transmission is used on the neonate's head for EEG signal transmission.

2.5 Machine Learning

These interpretable Artificial Intelligence (AI) models are made up of two main modules. First, the feature extractor module pre-processes the EEG signal and identifies characteristics of the EEG signal which are the input to the classifier. Secondly the interpretation model. [25] have done a review of the developed AI models and the datasets they used to train and test the models. [26] have introduced a Convolutional Neural Network (CNN) to detect seizures with a cross-validation approach. They have two convolutional layers with max pooling layers. [27] developed a model with a support vector machine(Support Vector Machine (SVM)) to identify neonatal seizures from EEG signals. [28] have developed a deep learning framework called STATEnet to identify neonatal seizures by the spatial-temporal features of multichannel EEG signals. On the other hand, [29] have done a systematic review of self-supervised contrastive learning for medical time series. Their study stated that self-supervised learning had been used to classify Motor-images, sleep stages, and seizures. [30] have developed a self-supervised learning model to detect epileptic seizures in adults. [31] and [32] have explained interpretations methods of the black box in a machine learning model in their respective studies and they have focused on Local Interpretable Model Agnostic Explanations (LIME) and Segmentation Class Activation Mapping (seCAM) methods.

Temko et.al [33] designed a support vector machine classifier for a dataset from Cork University Maternity Hospital. With the recent advancements in deep learning with deep CNN, RNN, and LSTM, several studies have been carried out to classify EEG signals. In [34, 35], they have applied 2D convolutions to detect seizures where in [35] the input EEG signal is treated as a 2D image, and in [34] the input is the spectrogram of the EEG epoch. In

the recent past, STATEnet [36] and ST-GAT [37] models have been introduced where the temporal and spatial features are considered for the model prediction. The main drawback of these existing models is that they are not scalable to a reduced number of channels. Also, their convergence is very slow and not able to explain the model output concerning the particular EEG channels and time intervals of the input EEG epoch. Michele et.al [38] have introduced an explainable deep learning model for blink detection from EEG using GRAD-Cam [39] method. We also apply a similar method but not the same as GRAD-Cam to explain the output of our model. Apart from these, some other studies in self-supervised learning(SSL) [40, 41] were conducted to detect seizures, but SSL is not performing well.

2.6 Signal Processing

EEG signals operate in the range $10 \mu\text{V}$ to $100 \mu\text{V}$ while the frequency ranges from 1 Hz to 100 Hz. Spectrum information extracted is used to decode brain activity by the sub-bands given by delta, theta, alpha, beta, and gamma. In the case of epilepsy, different frequency spectra for several states can be identified as post-ictal, ictal, and prodrome[42]. In the ictal state, it can be identified that there's a higher energy distribution in frequency ranges from 0 Hz to 40 Hz. It can also be seen that there's a peak occurring at 6 Hz[26].

Since EEG signals are measured at the scalp the brain wave strength drops to 5% in EEGs. Therefore, removing noise and improving Signal to Noise Ratio (SNR) is done before analysis[42]. The origin of this noise can be random noise and various artifacts generated through amplifiers, cables, or motions such as eye movements. Because of the low amplitude of EEGs, they are affected through these sources. Basic filtering methods such as Kalman filters or Chebyshev filters can be used to remove random noise. Smoothing filters such as the Savitzky–Golay filter have been used as well to improve the signal quality [43].

Removing artifacts has been discussed under methods such as Wavelet Transform, Independent Component Analysis, Empirical Mode Decomposition, Time-Frequency Image Dimensionality Reduction, Neural Networks, and several hybrid methods involving Wavelet decomposition and independent component analysis, which is the widely popular method. The main advantage of Independant Componenet Analysis (ICA) is the interpretability (ability to analyse which) components were identified as noisy.

IC classifiers are typically done using the following features,

- Temporal Data
- Power Spectral Density (PSD) Data
- Topological Maps of Independent Components (ICs)

These were used as handcrafted features in several past researches. [44] had used handcrafted spatial, spectral and statistical features, [45] discusses a method called FASTER which uses features such as channel variance, [46] brings out a method called TDSEP which uses a temporal correlation, [47] uses temporal and spatial features in a method called ADJUST, [48] uses multinomial regression to classify independent components, while [49] uses 10 SVMs to classify artifacts.

However, recent publications such as[50] show Deep Neural Network (DNN)s allow for featureless models with higher accuracy for artifact classification.[51] shows two models, ICAlabe and ICAlabel_{*lite*}, with the later showing faster accuracy. This was a 13 times faster algorithm and trained using 200000 independent components from 6352 EEGs and classified into several subcategories (brain, muscle, eye, heart and line noise). [52] shows Bayesian deep learning and attention modules to increase accuracy. [53] uses a dataset called EPIC [54] extracted using another EEG dataset called EPILEPSIAE [55] which contains EEG data of patients having epileptic seizures.

Chapter 3

Methodology

3.1 Overview

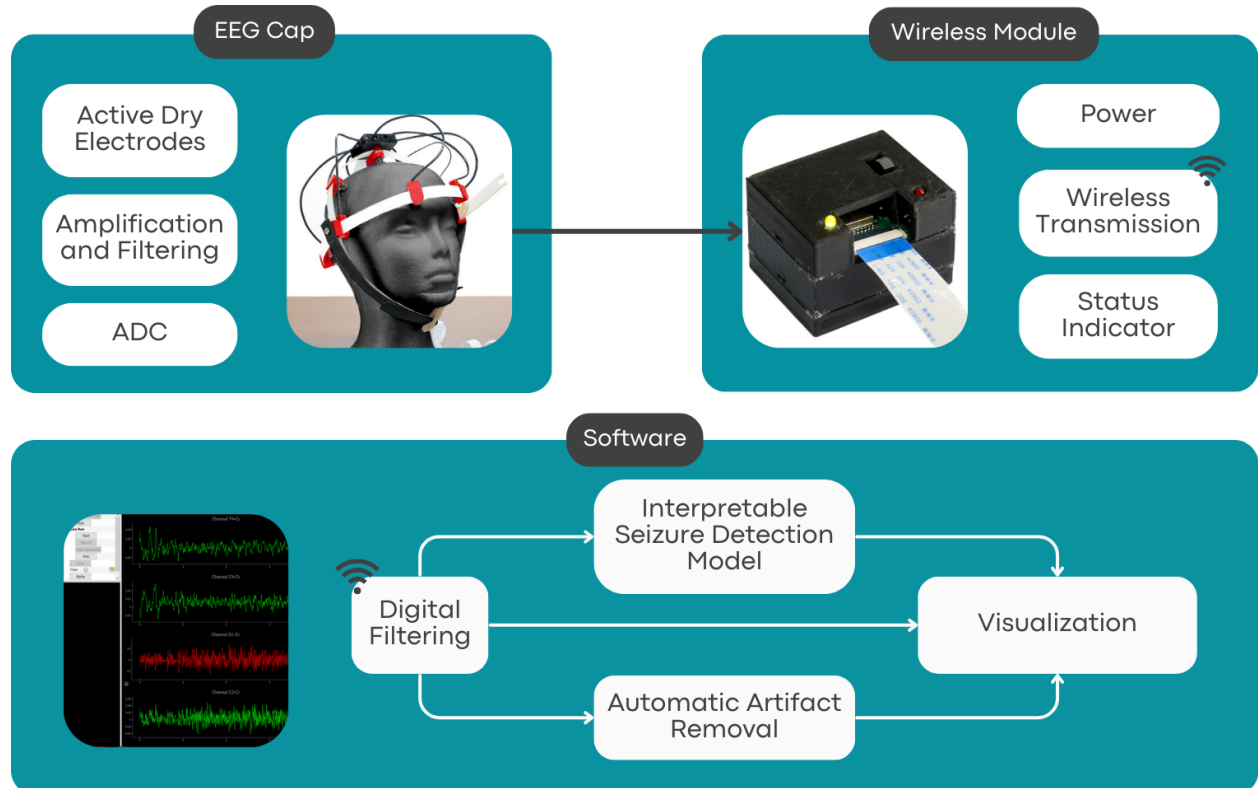


Figure 3.1: Overall block diagram

This work proposes a comprehensive system for EEG signal acquisition and analysis, particularly targeted towards neonatal seizure detection. The system comprises a:

1. Hardware Interface:

- Active electrode design for signal conditioning
- Analog Front End (AFE) for analog to digital conversion of EEG signals with an integrated IMU
- Microcontroller unit for interfacing ADS1299 IC, IMU sensor and status indicator which also facilitates wireless data transmission
- Highly adjustable headset design to hold all the hardware elements together

2. Software Interface:

- Real-time interpretable seizure detection model
- Automatic artifact removal algorithm
- Graphical User Interface (GUI) to monitor EEG signals and incorporate all the above elements together

The following sections will delve deeper into the methodologies used in each of these components.

3.2 Hardware

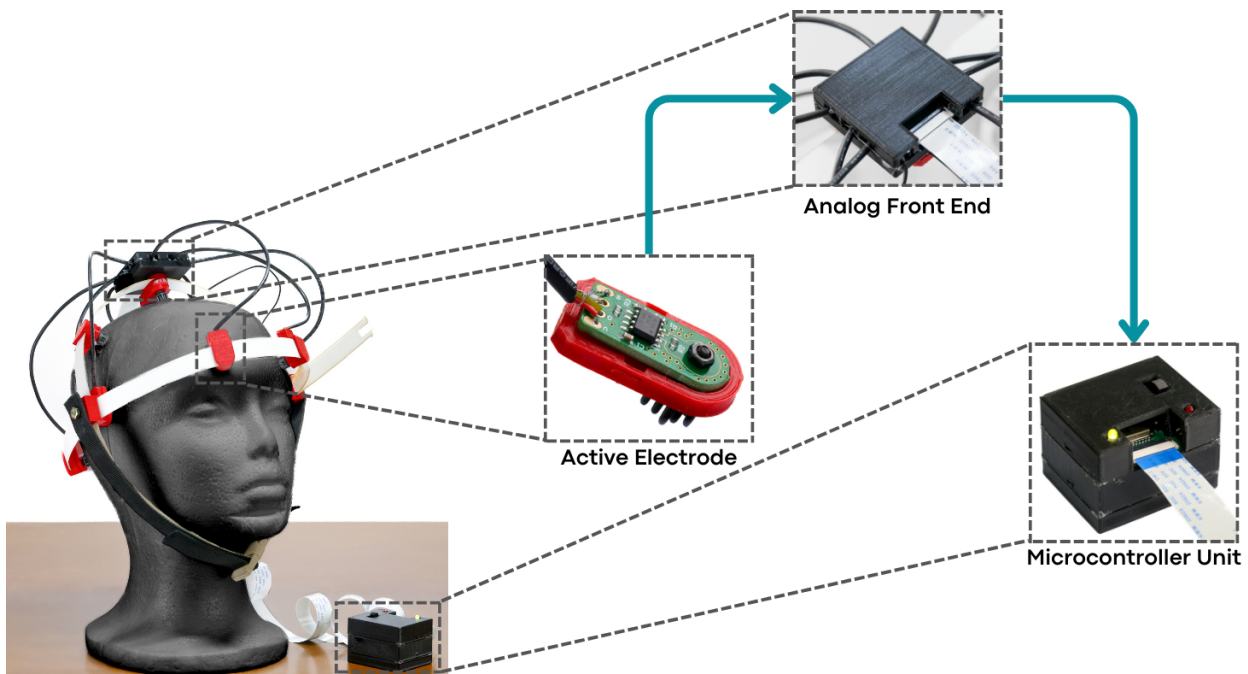


Figure 3.2: Hardware block diagram

3.2.1 Headset Design

The final headset design was a result of improvements done on different designs after identifying the practical issues with them. The electrodes which capture the EEG signals are attached to the headset. The placement of the electrodes can be changed slightly by sliding them along the strips, so it has the ability to cater to varying head shapes and sizes. The headset design uses the reduced electrode montage with 8 electrodes, reference and ground to capture the EEG signals.



(a) Mark I Design



(b) Mark II Design



(c) Mark IV Design



(d) Mark IV Design

Figure 3.3: Different headset designs tried throughout the project

Mark I Design: In this design, non-elastic fabric strips were used to slide the electrodes. A 3D-printed plastic buckle was used to attach the fabric straps. Sliding the electrodes on the fabric strips was harder and adjusting the strip length from user to user was also not very convenient in this design. As this design did not have any chin strap, placing the headset steadily could not be done.

Mark II Design: The non-elastic fabric strips were replaced by elastic fabric strips. A chin strap locked by a plastic buckle was also used. As it was based on the fabric strips, it did not have any defined shape. Hence, the straps tended to tangle easily.

Mark III Design: Here, 3 flexible plastic strips with holes with a gap of 0.5cm were used to slide the electrodes with a chinstrap. A plastic buckle with an angular base was used

to adjust the strip length, but without a locking mechanism, the strips often detached and broke due to the brittleness of the plastic.

Mark IV Design: Plastic strips attached to three Velcro fabric strips and a Velcro headband were used in this design, without a chin strap. The addition of plastic strips added rigidity to the device, preventing the Velcro from tangling. The strips did not fix well, as they were attached to the headband around the same area.

Mark V Design: In this design, two plastic strips are used to slide the electrodes to the relevant location. One strip is around the head like a headband where the electrodes for O1, O2, Fp1 and Fp2 positions are slid on it. The other plastic strip goes over the head and facilitates the C3, C4, T3, T4 and Cz electrodes. The Cz electrode, which is on the top of the head is directly attached to the Analog Front End, which is also slid on this strip. The length of the plastic strips is adjustable. After setting the relevant strip length according to the user's head shape, they are tightened using two hex head bolts. An adjustable-length chin strap with a plastic buckle was also used to tighten the headset for better signal acquisition.



Figure 3.4: Final EEG headset design

3.2.2 Electrode Design

Attached to the headset are the electrodes of the device. The electrodes are used to capture the EEG signals from the subject. Active electrodes were designed to capture EEG signals with higher quality. Several design considerations and features of the electrodes are given below.

Electrode: Ag/AgCl multi-spike-shaped dry electrodes are used as the electrode of the design. Ag/AgCl was selected as the material due to its high conductivity and relatively low

cost. Multi-spike-shaped electrodes were used so the electrodes would contact well with the head despite the hair.

PCB Design: The PCB of the electrode consists of two layers, both in ground voltage. The Ag/AgCl electrode is in direct contact with the PCB by a pad. All components soldered are SMD components.

Gold-plated: Instead of the copper pads in conventional PCBs, here we use Gold-plated pads. These are used for higher-quality signal acquisition as well as corrosion resistance.

Shielding: Shielding is done to reduce the external noise interferences to the EEG signal acquisition process. In the electrode design, shielding is done at the PCB as well as off the PCB. Via stitching and guard ring techniques are used in the PCB. Active shielding is done to the cable where data is transmitted from the active electrode to the analog front end.

Low Noise Buffering and Signal Conditioning: Captured EEG signal is buffered using an OPA2376AIDR operational amplifier which has high precision, high input impedance, and low-noise properties. As an added feature, this op-amp contains EDS protection as well.

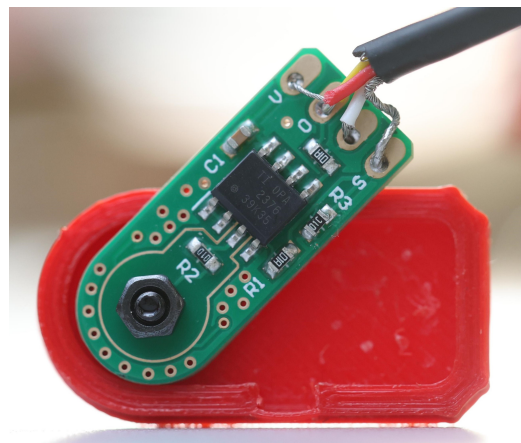


Figure 3.5: Designed active electrode used for EEG signal acquisition

The schematic diagram and PCB design of the Active Electrode can be found in the Appendix.

3.2.3 Analog Front End

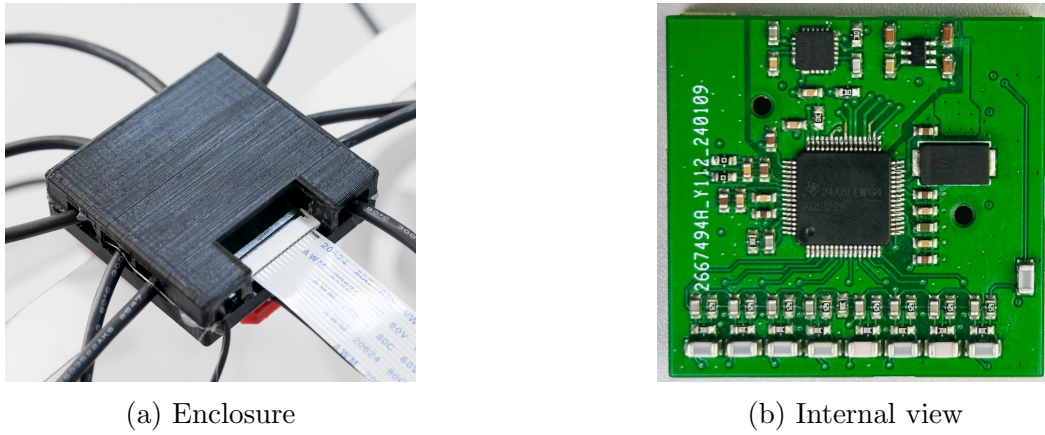


Figure 3.6: Analog front end

The AFE is a critical stage in processing the conditioned EEG signals from the active electrodes. It ensures high-fidelity capture while minimizing noise and preparing the signal for digital conversion.

Mark I - Breadboard Design

To ensure high-quality signals we use the ADS1299 IC as the main component in our AFE. Initially, it was necessary to configure and interface the ADS1299 IC. For this, we used a 64-pin QFP to DIP converter to test the ADS1299 IC. The breadboard design is shown in Figure 3.7. The results obtained using this method added a lot of noise due to the large number of tangled wires. The results obtained using this method are shown in Figure 3.8

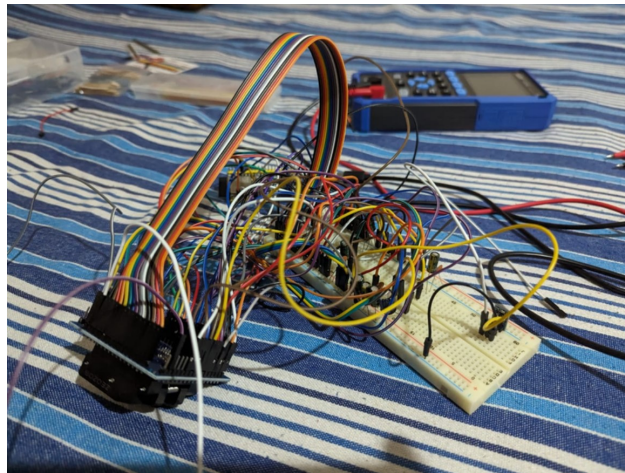


Figure 3.7: Breadboard design

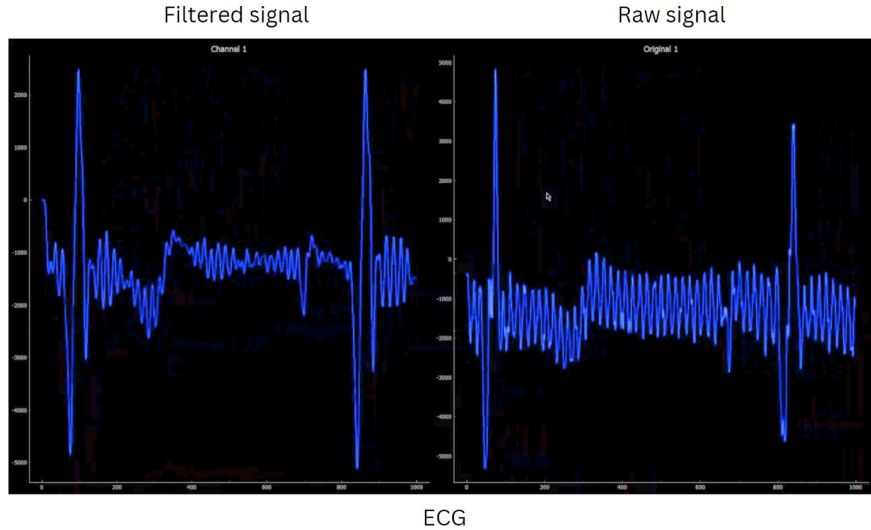


Figure 3.8: Results from the breadboard design

Mark II - Dotboard Design

After testing the functionality of the ADS1299 IC using the breadboard design, a dotboard design was implemented for further testing. This reduced the number of coupled wires and made the design much more compact and reduced the noise levels further. The dotboard design and the results obtained using this method are shown in Figure 3.9 and Figure 3.10 respectively.

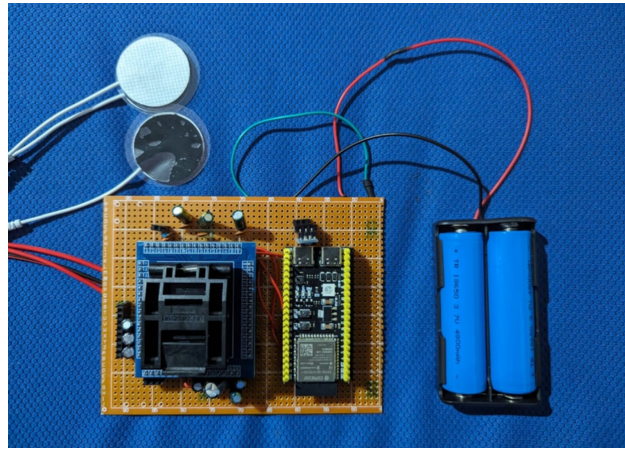


Figure 3.9: Dotboard design

Mark III - PCB Design

The final design included a number of design considerations to ensure minimal noise in the system. A breakdown of the key components in the final design is described below.

Isolated Ground Planes: The AFE utilizes separate ground planes for analog and dig-

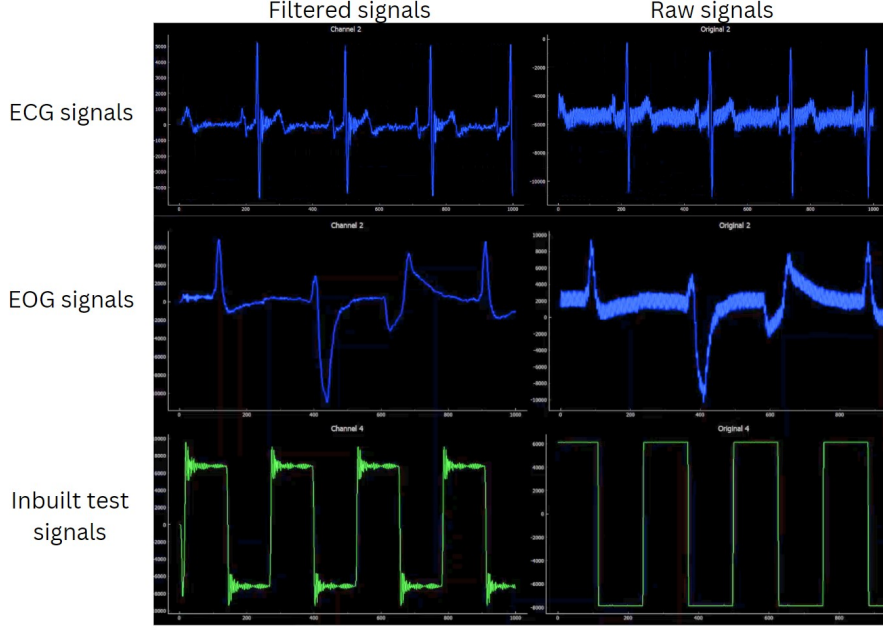


Figure 3.10: Results from the dotboard design

ital signals connected at a single point. This physical separation minimizes noise coupling between the sensitive EEG signals and the high-frequency digital processing circuitry.

Filtering: A high-pass filter with a 0.1 Hz cutoff frequency is used to remove slow drifts and baseline wander from the EEG signal, preventing saturation of the amplifier. A low-pass filter with a 120 Hz cutoff frequency is used to eliminate high-frequency noise beyond the EEG bandwidth (typically above 100Hz) to prevent aliasing during digital conversion.

High-Quality Capacitors: Class 1 Multilayer Ceramic Capacitors (MLCC) are used throughout the filtering and power decoupling stages. These capacitors offer low equivalent series resistance (ESR), excellent stability, and low piezoelectric effect, minimizing noise introduced by the capacitors themselves.

ADS1299 Integrated Circuit (IC): This is the main component of the AFE. It's a low-noise, 8-channel, 24-bit Analog-to-Digital Converter (ADC) specifically designed for EEG applications. Key features of this IC are highlighted below:

- Low noise
- 8-channel
- 24-bit ADC
- 1-24x Programmable gain amplifier
- Internal Driven Right Leg (DRL) circuit for increased common mode rejection
- 250Hz sampling rate suitable for EEG signal capture
- SPI communication interface for interfacing with the digital processing unit

IMU Sensor (MPU6050): A 6-axis Inertial Measurement Unit (IMU) sensor is integrated to capture head movement data. This data can be used to identify movement artifacts in

the EEG signal.

Power Supply (LTC19285): A dedicated low-noise doubler charge pump (LTC19285) provides a clean and boosted voltage supply specifically to power the ADS1299 IC.

Small and Lightweight: AFE is lightweight to ensure comfort to the user when worn on the head.

By combining these components, the AFE effectively converts the raw EEG signals to a digital format, enabling accurate analysis and interpretation in the later stages. The schematics and PCB design of the AFE can be found in the Appendix.

3.2.4 Microcontroller Unit

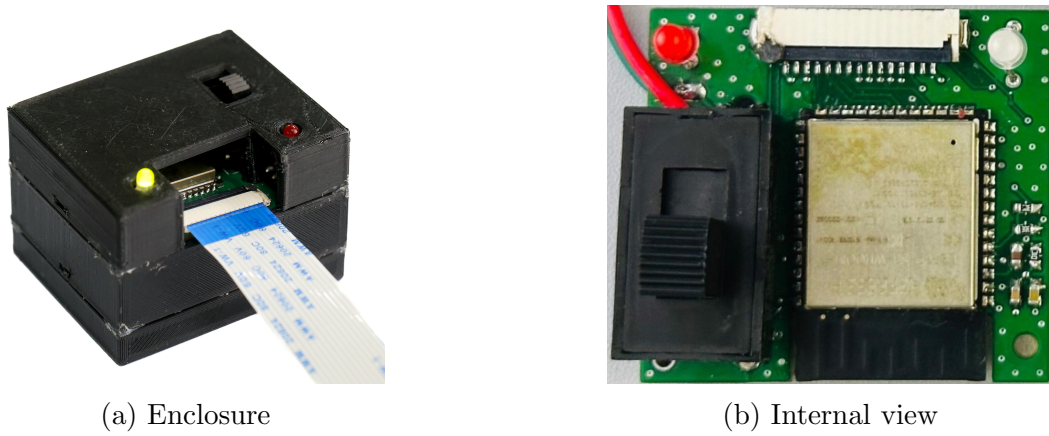


Figure 3.11: Microcontroller unit

The microcontroller unit facilitates data transmission from the device to the computer wirelessly. The microcontroller unit receives data from the analog front end via a flexible flat cable. An ESP32-S3 is used as the main microcontroller of the device. Several design considerations and features of the microcontroller are given below.

PCB Design: The PCB of the microcontroller unit consists of 4 layers. A cut was made in the PCB at the antenna of the ESP32-S3 module antenna to reduce interference for data transmission.

Status Indicating LED: Two LEDs are used in the microcontroller unit. They are used to give an update of the current working state of the device. Here blinking LED indications are used for the processes which run for a long time to save battery.

USB Debugging: The device has the capability to debug firmware code using a micro-USB port. This can be done to both ESP32-S3 on the microcontroller unit as well as the ADS1299 of the analog front end.

Data Transmission: The EEG signals are transmitted to the computer through 2.4 GHz Wi-Fi signals generated by the ESP32-S3 at a rate of 250Hz. The TCP protocol is used in this regard due to the low level of packet loss.

Table 3.1: Different status indicated by the LEDs

Status	LED and Color
Working Device Indications	
Initial device startup	Status Indicator - Red
Initialize Wi-Fi and ADS1299	Status Indicator - Green
Connected to Wi-Fi	Status Indicator - Orange
Data transmitting	Status Indicator - Green blinking
Battery Indications	
Battery charging	Charging Indicator - Red
Battery fully charged and device off	Both LEDs off
Low battery (20%)	Status Indicator - Red blinking

Battery: A rechargeable 2000mAh, 3.7-4.2V Li-Po battery is used as the power supply of the device. It is kept inside the same enclosure as the microcontroller unit. It can be charged using the micro-USB port.

USB Isolator: The device can only be charged when power is off, and it will not be charging when the device is in use. This safety feature is performed by a USB isolator. Due to this, the patient will never get exposed to the main powerline.

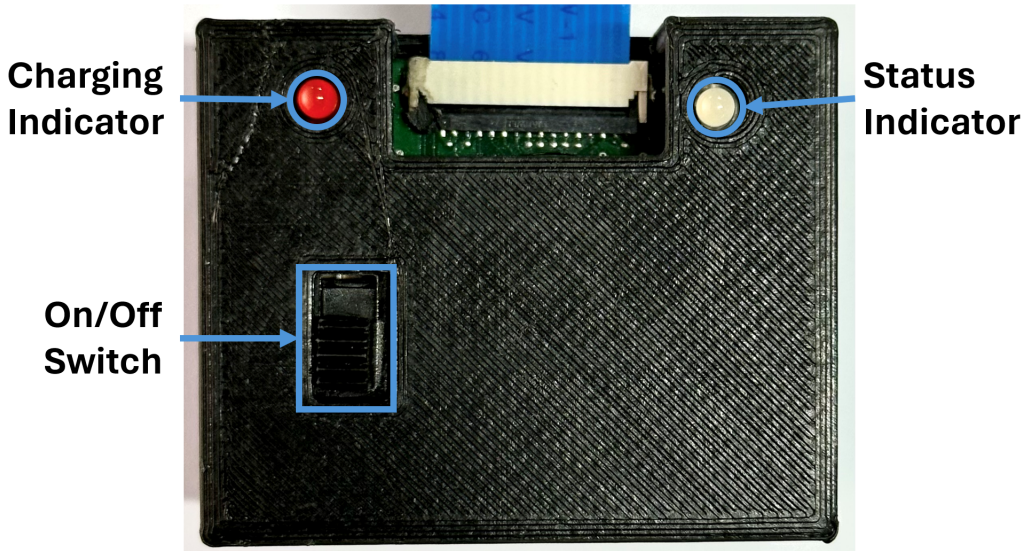


Figure 3.12: Microcontroller unit design

The schematics and PCB design of the Microcontroller unit can be found in the Appendix.

3.2.5 Total Cost of Product

The total cost of the product can be categorized as shown in Table 3.2

Table 3.2: Cost breakdown for the product

Component	Price (US \$)
Analog Front End	
ASD1299	58.43
MPU6050	7.74
Other Electronic Components	9.26
PCB Printing	1.40
Enclosure 3D Printing	0.50
Total for 1 AFE	77.33
Microcontroller Unit	
ADUM4160	4.53
ESP32-S3	3.90
Li-Po Battery	2.20
Other Electronic Components	6.78
PCB Printing	1.40
Enclosure 3D Printing	0.50
Total for 1 MCU	19.31
Active Electrode	
OPA2376AIDR	2.74
Other Electronic Components	0.34
PCB Printing	2.08
Shielded Cables	0.10
Enclosure 3D Printing	0.10
Total for 9 Electrodes	48.24
Headset Design	
Material Cost	1.00
3D Printing of Electrode Sliders	0.50
Total for 1 Headset	1.50
Total for 1 Full Product	146.38

3.3 Software

This section is dedicated to discussing the significance of signal processing, machine learning approaches, and having a GUI to display real-time signals. As discussed in chapter 2, several studies have been conducted to analyze and classify EEG signals. In this study, we propose new algorithms to analyze publicly available pre-recorded EEG datasets and EEG signals acquired from our device described in 3.2. The following diagram 3.13 shows a complete software block diagram.

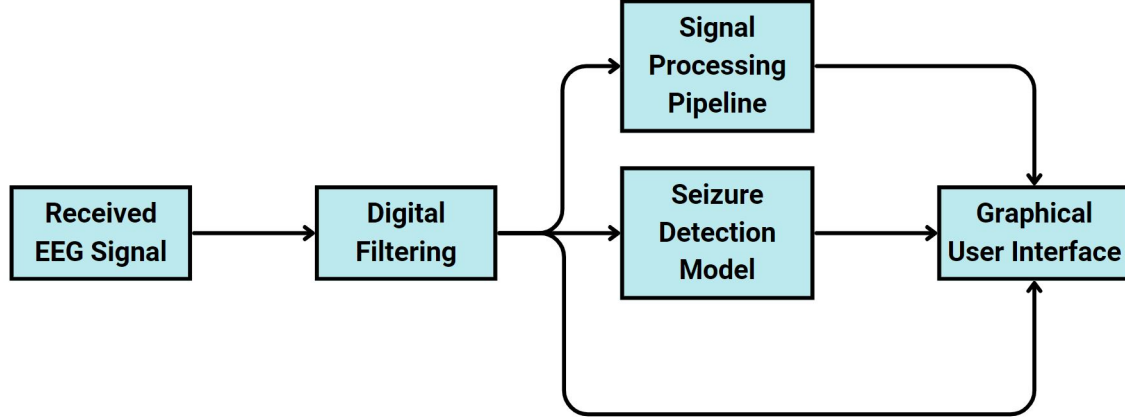


Figure 3.13: Software block diagram

3.3.1 Machine Learning

Dataset and Preprocessing

In this study, the publicly available Helsinki Zenodo scalp electroencephalogram(EEG) dataset [56] is used to train and test the deep learning model. This dataset was recorded from 79 term neonates admitted to the Neonatal Intensive Care Unit (NICU) at Helsinki University Hospital. It consists of three annotation files created by three independent neurologists. As a result, only 39 neonates were identified as having seizures by consensus, while 22 were identified as seizure-free.

This dataset, recorded with respect to a reference point, allows for the construction of a number of EEG channels. Consequently, most existing methods, including the state-of-the-art, utilize 18 EEG channels for training and evaluation. However, this study employs only 12 channels, selected based on Hasan et al.[57] to model the double banana-shaped electrode montage. The specific channels used are, Fp1-T3, T3-O1, Fp1-C3, C3-O1, Fp2-C4, C4-O2, Fp2-T4, T4-O2, T3-C3, C3-CZ, CZ-C4, C4-T4 (see Figure 3.14a)

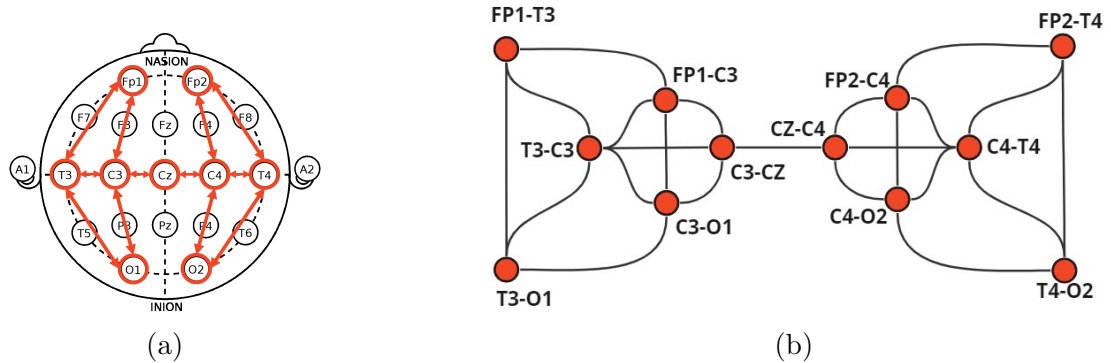


Figure 3.14: (a) The illustration of employed reduced electrode montage Graph representation of the selected electrode montage. (b) Node represents the channels and edges represent the functional connectivity between channels.

Signal preprocessing plays a crucial role when it comes to EEG signals due to their added noise and artifacts. Additionally, in this dataset, some EEG signals exhibit flat lines at 0V, necessitating their removal before applying further processing techniques. We implemented an automated procedure to remove these flat lines from the signals only if all selected channels within a specific time range contain flat lines. Subsequently, a bandpass Chebyshev type II digital filter with cutoff frequencies of 1 Hz and 30 Hz was applied forward and backwards signals to eliminate baseline drift and high-frequency noise components, including power line noise. Considering that the deep learning model utilizes 12-second EEG epochs, maintaining the original sampling frequency of 256 Hz would significantly increase model complexity and training and inference times. Therefore, as in [33], all signals were down-sampled to 32 Hz.

We selected only the 39 neonates with seizures identified by consensus to train and evaluate our model as the other 22 neonatal seizure-free signals cause huge class imbalance issues and the remaining 18 neonatal signals have the potential to misclassify actual seizures. Although neonates with seizures by consensus were selected, there was a significant difference in total seizure duration compared to non-seizure duration. The total seizure duration represents only 18.14% of the total EEG signal duration. To address this class imbalance issue, we adopted a technique from [37], we overlap each 12-second epoch with 11 seconds for seizure segments and 10 seconds for non-seizure segments. While this approach doesn't entirely eliminate the class imbalance, it effectively reduces its impact displaying a seizure to non-seizure epochs ratio of 1:2. This issue is totally solved with the loss function.

Machine learning is a very powerful tool in the automation of many human resource-intensive tasks. Therefore we can see machine learning in many real-world applications namely robotics, the health sector, autonomous vehicles, and many other newly emerging fields. If we particularly focus on machine learning for the healthcare sector we can see a lot of applications including biosignal processing and medical image processing. Therefore in this study, we discuss machine learning and deep learning approaches for biosignal processing and classification.

First, we designed a big CNN same as the ResNet50 model but with 1D convolutions. We trained this network with 4-second EEG epochs without preprocessing the signals. Our main aim with this model was to check if we could at least train a model to discriminate between seizure and non-seizure epochs. This was a successful initial step but the problems with this model were high training time even on GPUs and quick overfitting to the dataset. Therefore we moved to developing another completely different small model to do our task. This second model was designed with 4 1D CNN layers and 3 fully connected layers. As you can see this is a very tiny model. All the layers in this model were followed by ReLu activation except the last dense layer which outputs Sigmoid values of the logit. This architecture was also trained with 4-second EEG epochs without applying any preprocessing technique. Because of that, the input size to the model was (12,1024). After several experiments with different model architectures, we finally decided to use the below-described architecture to detect seizures from EEG signals.

After that, as an alternative approach, we trained a self-supervised learning algorithm to improve the performance of the suggested model. In this case, we relied on contrastive learning for training the model in the upstream task. For that, we had to apply strong data

augmentation to reduce the training loss. So, here onwards we are going to deeply discuss our final employed Machine learning model.

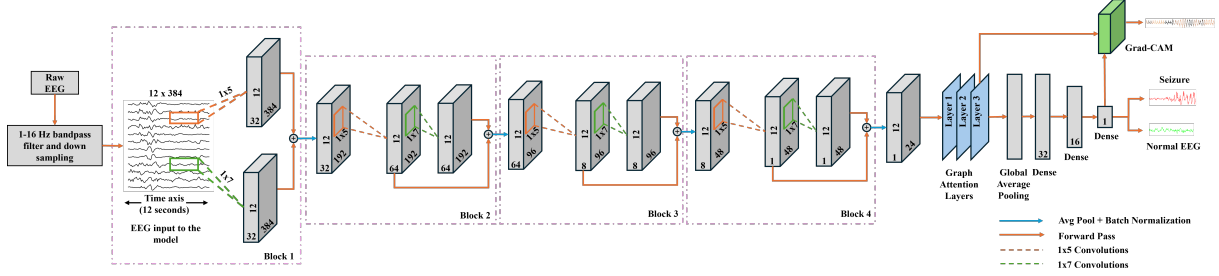


Figure 3.15: Full deep learning model

Finalised Deep Learning Model Architecture

Training an AI model for neonatal seizure detection is a tedious task even with the available annotated datasets, as seizure duration is often shorter than overall signal recording. To address this challenge, we introduce a new deep-learning model (figure 3.15 for real-time seizure detection from neonatal EEG signals. Our model employs a CNN encoder, a graph attention encoder, and a fully connected classification head. The CNN encoder is used to extract the temporal features from the EEG epochs and the graph attention encoder is used to extract spatial features from the output of the CNN encoder. Apart from seizure detection, notably, we integrate interpretability in our model to explain which channels and time ranges of a given EEG epoch contribute more significantly to the model output.

CNN Encoder

CNNs are widely applied in computer vision [58, 59] and sequence transduction [60, 61] tasks, serving as the main architecture in many models. Therefore, in this study, as the EEG signals are sequential data, we used 1-D convolutions to extract temporal features from EEG epochs. Our CNN encoder was designed with four blocks as shown in figure 3.16. Each block has 2 convolution layers with zero padding and stride 1 with either (1×5) or (1×7) receptive fields(kernel size). Also, we apply $\{32, 64, 8, 1\}$ filters in blocks 1,2,3 and 4 respectively, as shown in the figure.

Let's consider $F(x, \{W_{1i}\})$ and $H(x, \{W_{2i}\})$ are two different mapping functions of some stacked layers that output two different matrices with the same dimension given the same input matrix x . Therefore, we are able to do two mappings parallelly and add them together to obtain a new matrix with completely different features as in the equation:

$$H(x, \{W_i\}) = F(x, \{W_{1i}\}) + H(x, \{W_{2i}\}) \quad (3.1)$$

We apply the same theory in the first convolution block as in Figure 3.16 to extract different temporal features at the same time by applying different kernel sizes in two convolutional layers. This block is followed by another three convolution blocks, each of them having a residual learning framework as proposed in [62] for fast convergence of the model. In our

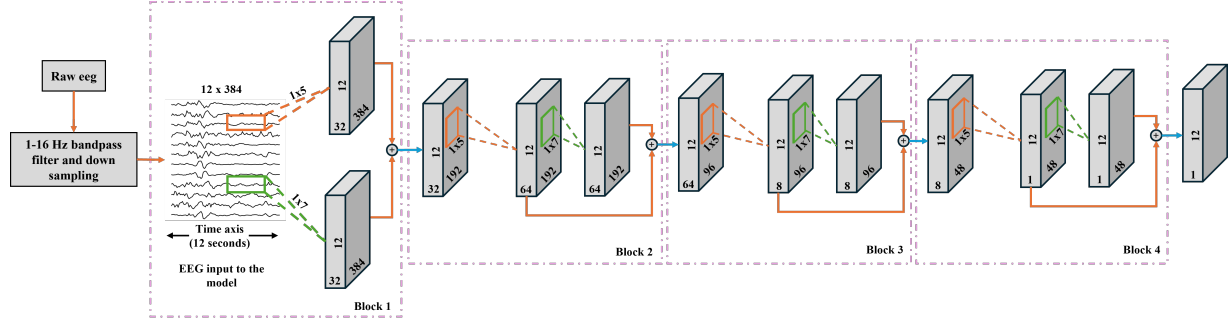


Figure 3.16: The first 4 blocks belong to the CNN-based temporal feature extractor. The 12 channels are preserved throughout the CNN encoder but down-sampled the temporal features at the end of each block using Average Pooling.

encoder, the skip connections simply perform identical mapping to preserve the original input dimensions when adding.

Although this encoder is a tiny network with only 8 convolution layers, it's hard to get at least a good training performance with a simple sequential network. Therefore, after several experiments, we came up with this well-performing encoder to extract the temporal features and dynamics from EEG signals. To introduce non-linearity in our model, we used rectified linear unit (*ReLU*) as the activation of each convolution layer because other activation functions may vanish the gradients in backpropagation or cause high training time and also, this is the widely used activation function in deep learning models. We also experimented with the *Swish* activation function but that increased the training time by approximately 13 minutes compared to the *ReLU* function.

After adding convolution outputs in each block, we perform average pooling to downsample the feature map by a factor of 2 for better optimization of the model and batch normalization as a solution to the gradient exploding issue according to [63]. The reason for using average pooling instead of max pooling is to aggregate more temporal information into one feature point rather than solely depending on a single value within a moving window.

Attention Encoder and Classification Head

Graph Representation: After extracting the temporal features from a signal, we need to extract spatial features from the EEG epochs with the help of inter-channel connectivity. Here, we employ a graph attention network [37, 64] to extract the spatial feature. To generate the graph, we need to know the vertices that correspond to the 12 channels, their feature vectors which are the output features from the CNN encoder for each channel, and the adjacency matrix to denote the functional connectivity between channel pairs. The selected channels as in the section 3.3.1, have the capability of modelling brain connectivity as in the graph in Figure 3.14b.

According to Hasan et.al in [57] the localization of EEG seizures with reduced electrode montage is acceptable and compared to a standard 10/20 EEG system. As most of the seizures occur in the central zone of the brain and as we have the local connections connecting

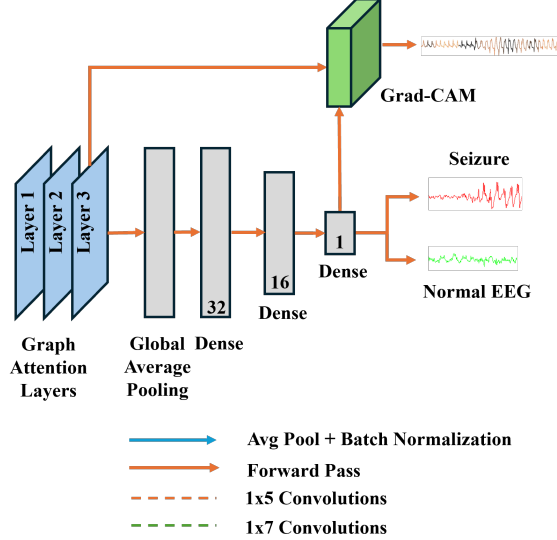


Figure 3.17: GAT layers 1, 2, and 3 have the output shapes (12×37) , (12×32) , and (12×16) respectively and the last MLP network has 32, 16, and 1 neurons respectively.

left and right hemispheres (horizontal line in the figure), not having global inter-hemisphere connections in the Front Lobe and Parietal Lobe doesn't reduce the network efficiency. Another fact is other neonatal seizures occur in bilateral posterior regions and bilateral anterior regions which are covered by O1, O2, Fp1 and Fp2. Also, due to the EEG channels T3-C3, C3-CZ, CZ-C4, and C4-T4, the biological connection between the left and right hemispheres is maintained throughout the process. Therefore, with the designed graph, it is possible to leverage the information passing between left and right parieto-occipital or fronto-temporal zones.

We did not rely only on this information, we experimented with several graphs and decided to employ this graph as it had less tendency to overfit the model and could achieve the best results.

Attention Layers: It is very important to pay attention to the connected EEG channels in the selected electrode montage when extracting spatial features. We had two options for the attention mechanism, either build an encoder employed by graph attention layers like in [37] or build an encoder with scaled dot product attention like in [65]. Though both perform in a similar way, GAT slightly outperforms dot-product attention as shown in the figure 3.18. Apart from this reason, the fact that using scaled dot product attention increases the number of learnable parameters and the brain network can be modelled as a graph, motivated us to apply a GAT encoder to extract spatial features.

In a GAT layer, each node aggregates features from adjacent nodes and constructs a new feature set for itself. Given the feature sets for each node $H \in \mathbb{R}^{12 \times F}$, a learnable weight matrix $W \in \mathbb{R}^{F \times F'}$ is required to linearly transform the input features to high-level features by the simple matrix multiplication $HW \in \mathbb{R}^{12 \times F'}$. Then a shared masked self-attention was performed to compute the attention coefficients and masking is done according to the

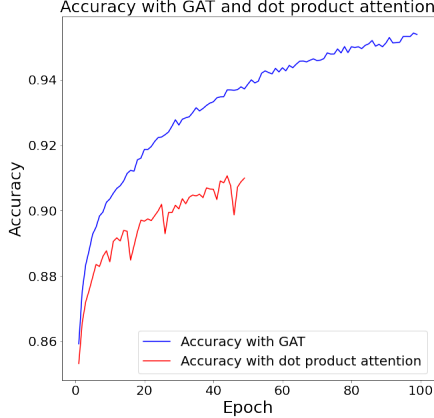


Figure 3.18: Performance comparison between GAT layers and scaled dot product attention layers. Training for dot product attention was terminated after 50 epochs as it has low performance

adjacency matrix. The equation 3.2 according to Peter. V et.al [64] explain how to compute the attention coefficients from the j^{th} node to the i^{th} node (α_{ij})

$$\alpha_{ij} = \frac{\exp(\text{LeakyReLU}([\vec{h}_i W || \vec{h}_j W] \vec{a}^T))}{\sum_{k \in \mathcal{N}_i} \exp(\text{LeakyReLU}([\vec{h}_i W || \vec{h}_k W] \vec{a}^T))} \quad (3.2)$$

Here \vec{h}_i denotes a row of H matrix, \mathcal{N}_i denotes all the neighbor nodes of node i and $a \in \mathbb{R}^{2F'}$ is a learnable weight vector. ($||$ represents concatenation). Once these attention coefficients are obtained, the new features set for each node are calculated by a simple linear transformation as in equation 3.3 which is followed by Exponential Linear Unit(Elu).

$$H' = \text{Elu}(H W \mathbf{A}) \quad (3.3)$$

Where $\mathbf{A} \in \mathbb{R}^{12 \times 12}$ is the masked attention coefficient matrix. This mask makes sure that a node pays attention only to itself and its first-order neighbours. Because of that, we apply three GAT layers after the CNN encoder, to achieve an optimal spatial receptive field by aggregating features from the third-order neighbors which will efficiently cover 78% of the brain network. The question here is, is it enough to apply only three layers? : Answer is yes. If we apply another one or two layers, the receptive field will be increased but it will not improve the network efficiency. This was proved experimentally, and the optimal number of Graph attention layers is 3. Here, the output feature matrices of the GAT layers 1,2 and 3 have the shapes (12×37) , (12×32) and (12×16) respectively. These values were used by Khadijeh et.al [37] in their paper.

After extracting temporal and spatial features from the proposed CNN and GAT encoders we perform the classification task through a fully connected classification head which consists of three dense layers of 32,16 and 1 neurons. The first and second dense layers are followed by the *ReLU* function while the final layer is followed by the *Sigmoid* function. Before this, the global average pooling layer is applied to reduce the dimensions.

Table 3.3: Model structure. N- Number of filters, K- kernel shape, W- Transformation matrix, a- shared attention vector. All Convolution layers use zero padding and stride 1

Layer/Block	Layer type	Parameters
Input		(12,384)
Convolution block 1	Convolution	K=(1,5),N=32, activation=ReLU
	Convolution	K=(1,7),N=32, activation=ReLU
	Add	-
	Average Pooling	K=(1,2)
	Batch Normalization	-
Convolution block 2	Convolution	K=(1,5),N=64, activation=ReLU
	Convolution	K=(1,7),N=64, activation=ReLU
	Add	-
	Average Pooling	K=(1,2)
	Batch Normalization	-
Convolution block 3	Convolution	K=(1,5),N=8, activation=ReLU
	Convolution	K=(1,7),N=8, activation=ReLU
	Add	-
	Average Pooling	K=(1,2)
	Batch Normalization	-
Convolution block 4 Reshape	Convolution	K=(1,5),N=1, activation=ReLU
	Convolution	K=(1,7),N=1, activation=ReLU
	Add	-
	Average Pooling	K=(1,2)
	Reshape	-
GAT 1 GAT 2 GAT 3	Graph Attention	W=(24,37) a=(74,1)
	Graph Attention	W=(37,32) a=(64,1)
	Graph Attention	W=(32,16) a=(32,1)
	Global Average Pooling	-
Fully connected network	Dense	K=32, activation=ReLU
	Dense	K=16, activation=ReLU
	Dense	K=1, activation=Sigmoid

Model Interpretability

When it comes to the medical domain, explaining the black box of the deep learning models is a must. This study proposes a new method based on gradient-weighted class activation mapping (Grad-CAM) [39]. In which the gradient of class activation is obtained with respect to the weights of the last GAT layer to generate a heatmap of the shape of the input signal. After finding the gradients, the final GAT layer outputs are scaled by the mean of gradients and sent through *ReLU* activation before normalizing. This algorithm is shown in algorithm 1

Algorithm 1 Real-time EEG seizure detection and explain the model output with a heat map

```
Model ← load the model
Model.trainable ← False
while Signal is received do
    X ← Read the EEG signal
    X ← Signal Preprocessing(X)
    GAT_output, model_output ← Model(X)
    Gradient ← 2D array (shape of X)

    for  $w_{i,j}$  in GAT_output do
        Gradient(i,j) ←  $\frac{\partial(\text{model\_output})}{\partial(w_{i,j})}$ 
    end for

    Heatmap ← GAT_output × mean of Gradient
    Heatmap ← resize the heat map to the shape of X
    Show the signal with the heat map

end while
```

Training and Hyperparameter Tuning

This section describes our model training and evaluation criteria. We trained the model on a Quadro RTX 5000, 16 GB GPU and for inferencing, we ran the model on an Intel® Core™ i7 – 10750H CPU. We trained and evaluated this model in two methods. The first one is allocating randomly selected 31 subjects for the training data set (80%) and the remaining 8 subjects for the test dataset(20%) from 39 neonates with seizures by consensus. Secondly, we performed 10-fold cross-validation on these 39 neonates. We trained the model for 50 epochs with 512 mini-batch size in each case and one epoch took a maximum of 45 seconds. Here, we applied Adam as the model optimizer with a 0.002 learning rate and had to apply Focal Binary cross entropy loss with $\gamma = 2$ and $\alpha = 0.4$ as the loss function to address the class imbalance issue between seizure and non-seizure samples. We apply several regularizations like dropout of 0.2 probability at the end of CNN block 1,2,3 and between every GAT layer and dense layer. Also, we use a L_2 kernel regularizer with a 0.0001 regularization value. We selected these hyperparameters after doing an ablation study.

3.3.2 Signal Processing

The entire architecture of the signal processing pipeline is indicated in the following 3.19 diagram.

Basic Preprocessing

Before removing artifacts, some basic preprocessing must be performed. The sources of noise occurrence are as follows:

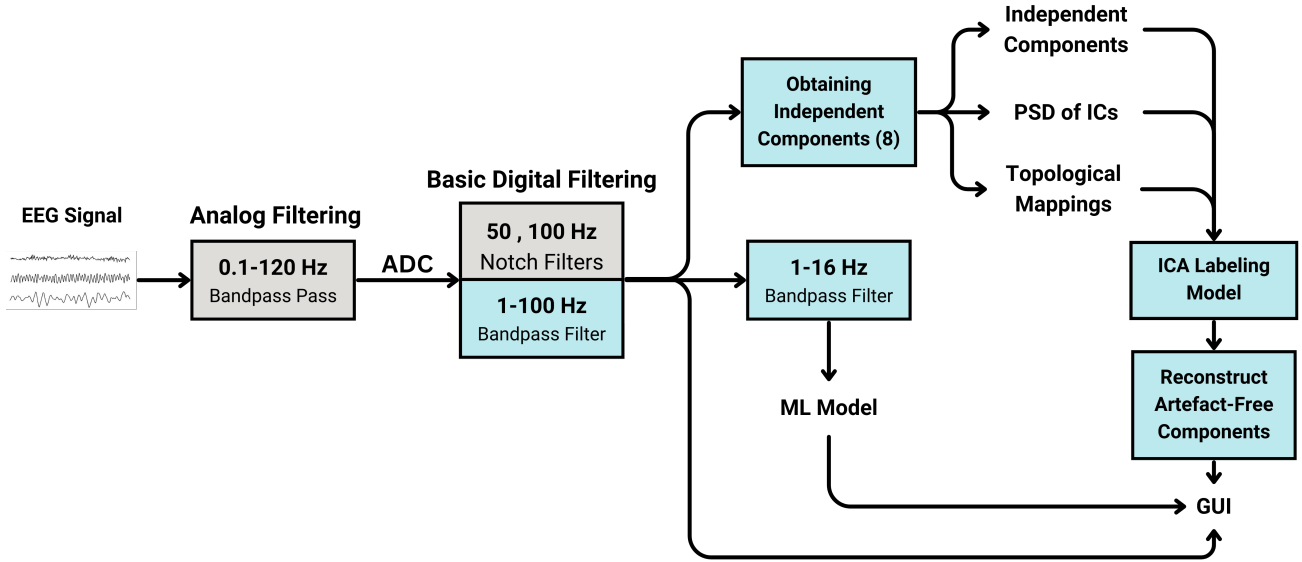


Figure 3.19: Signal processing pipeline

- Baseline drift: $0.001 - 0.5$ Hz
- Powerline noise: 50 Hz
- Muscular artifact and other high-frequency noises: ≥ 50 Hz

A 4th-order Butterworth bandpass filter ranging from 1 to 100 Hz is used to eliminate these noise components. Additionally, second-order 50 Hz and 100 Hz notch filters are also used.

Artifact Removal

EEG signals are often contaminated with noise from various sources, such as muscle artifacts and eye blinks. Researchers consider ICA a commonly used method to eliminate these noise artifacts from EEGs. This method separates the signal into multiple sources but requires visual inspection of data, which is time-consuming and requires experts. As noted in the literature review, deep learning approaches have outperformed manually extracted feature models because DNNs can directly extract complex non-linear data. Our methodology uses the architecture proposed by [53], slightly improving the independent component label classification model. We used the EPIC[54] dataset, which contains data from the EPILEPSIAE [55] data set and data from epileptic patients, to ensure that our algorithm doesn't identify seizures as artifacts.

Extended-Infomax ICA

In EEG artifact removal, we typically take the following assumption into account; the measured cerebral activity, denoted as \mathbf{x} , is viewed as the sum of cerebral and noise activity (artifacts). This is represented by

$$\mathbf{x} = \mathbf{A}\mathbf{s} \quad (3.4)$$

where \mathbf{A} is considered the mixing matrix.

Blind Source Separation (BSS) aims to estimate \mathbf{s} from the observations of \mathbf{x} , utilizing the information provided by all the electrodes. The objective of ICA is to discover the source signals so that,

$$\mathbf{s} = \mathbf{W}\mathbf{x} \quad (3.5)$$

where \mathbf{s} are statistically independent source mappings and \mathbf{W} is the unmixing matrix.

The mutual information (obtained from Kulbeck-Leibler divergence),

$$I(\mathbf{x}) = \int \rho(\mathbf{x}) \log \left(\frac{\rho(\mathbf{x})}{\prod_{i=1}^N \rho_i(x_i)} \right) d\mathbf{x} \quad (3.6)$$

of these sources are 0 only when the sources are independent. Here, $\rho(\mathbf{x})$ represents the multivariate Probability Density Function (PDF) of the sources and can be modelled as a product of all the marginal distributions of \mathbf{s} ($\rho_i(s_i)$) as below.

$$\rho(\mathbf{s}) = \prod_{i=1}^N \rho_i(s_i) \quad (3.7)$$

The learning algorithm uses the maximum log-likelihood function,

$$L(\mathbf{u}, \mathbf{w}) = \log |\det(\mathbf{W})| + \sum \log p_i(\mathbf{u}_i) \quad (3.8)$$

where \mathbf{u} relates to the hypothesised distribution of \mathbf{s} . The purpose of extended-infomax is to separate sources with different distributions like sub and super-Gaussian distributions. To do this they adapt 2 learning rules for sub and super-Gaussian distributions indicated as below. [66]

$$\Delta \mathbf{w} \propto \begin{cases} \mathbf{I} - \tanh \mathbf{u} \mathbf{u}^T - \mathbf{u} \mathbf{u}^T & : \text{supergaussian} \\ \mathbf{I} + \tanh(\mathbf{u}) \mathbf{u}^T - \mathbf{u} \mathbf{u}^T & : \text{subgaussian} \end{cases} \quad (3.9)$$

ICA Labeling Pipeline

The methodology described in the subsection above employs the extended-infomax algorithm in the `mne` library to obtain the sources, unmixing, and mixing matrices. The independent component label model used to label these independent components has been trained using the EPIC dataset. To label the independent components, the model inputs the time series EEG independent component, PSD of the EEG independent component, and topological mappings of each IC.

Topological plots are scalp topographies that show how each independent component maps into each electrode on the subject's scalp. The fixed points in the topograph correspond to each column of the mixing matrix[67]. Topoplots are generated with a resolution of 67x67. The algorithm used to generate these plots is similar to the topoplot function in EEGLAB[68], using inverse distance for interpolation, unlike the cubic interpolation in the `mne-ICAlabel` library. The circular mask is given to the mean of the mixing matrix columns. The channel locations are read according to the 10-20 electrode system.

The PSDs consist of 67 data points using the periodogram function in the `scipy` library. The time series data consists of 2-minute epochs of 256 Hz sampled data. More information regarding the used dataset can be found in the next section.

These features (8 channels corresponding to the channels - “T4” , “Fp2” , “C4” , “O2” , “O1” , “Fp1” , “C3” , “T3” in order) are input to the independent component label model. The independent components with noise as the label are zeroed, and then the vectors are mixed to obtain the cleaned EEG signal.

$$\mathbf{x}_{\text{clean}} = \mathbf{W}^{-1} \mathbf{s}_{\text{clean}} \quad (3.10)$$

The independent components with the brain as the label is zeroed to obtain the artifact signal as the output.

$$\mathbf{x}_{\text{noise}} = \mathbf{W}^{-1} \mathbf{s}_{\text{noise}} \quad (3.11)$$

This approach helps to identify the independent components that contain noise and separate them from the independent components that contain the brain’s electrical activity. Ultimately, it enables us to obtain a cleaner EEG signal, which is critical for accurate analysis of brain activity.

The EPIC Dataset

The EPIC dataset comprises annotated independent components extracted from the EEG recordings of patients diagnosed with epilepsy. It contains 77,426 independent components extracted from 613 hours of EEG data. These recordings consist of 19-channel EEGs sourced from the EPILEPSIAE dataset, with a sampling frequency of 256 Hz. Notably, the dataset captures day-to-day artifacts such as eating and sleeping, which are common occurrences in patients undergoing pre-surgical evaluation. The dataset includes recordings from 25 patients, comprising 13 males and 12 females. Corresponding time series data and topographic maps accompany each independent component within the dataset. Further, the independent components are categorized into two classes: brain and noise. The brain label contains 43,038 training data files and 11,437 testing files, while the noise label contains 18,054 training files and 4,897 testing files.[54]

IC Model Architecture

The architecture is an ensemble of DNNs and this contains 3 parallel DNNs for each input feature.

- For time series data - A BiLSTM to extract temporal features from the IC time series
- Two CNNs to extract spatial and temporal features from PSDs and topological plots

In the temporal feature extracting encoder, six 1D convolution layers (from 4-128 filters) are used to extract temporal features from the data. All the filters are of size 3×1 and stride

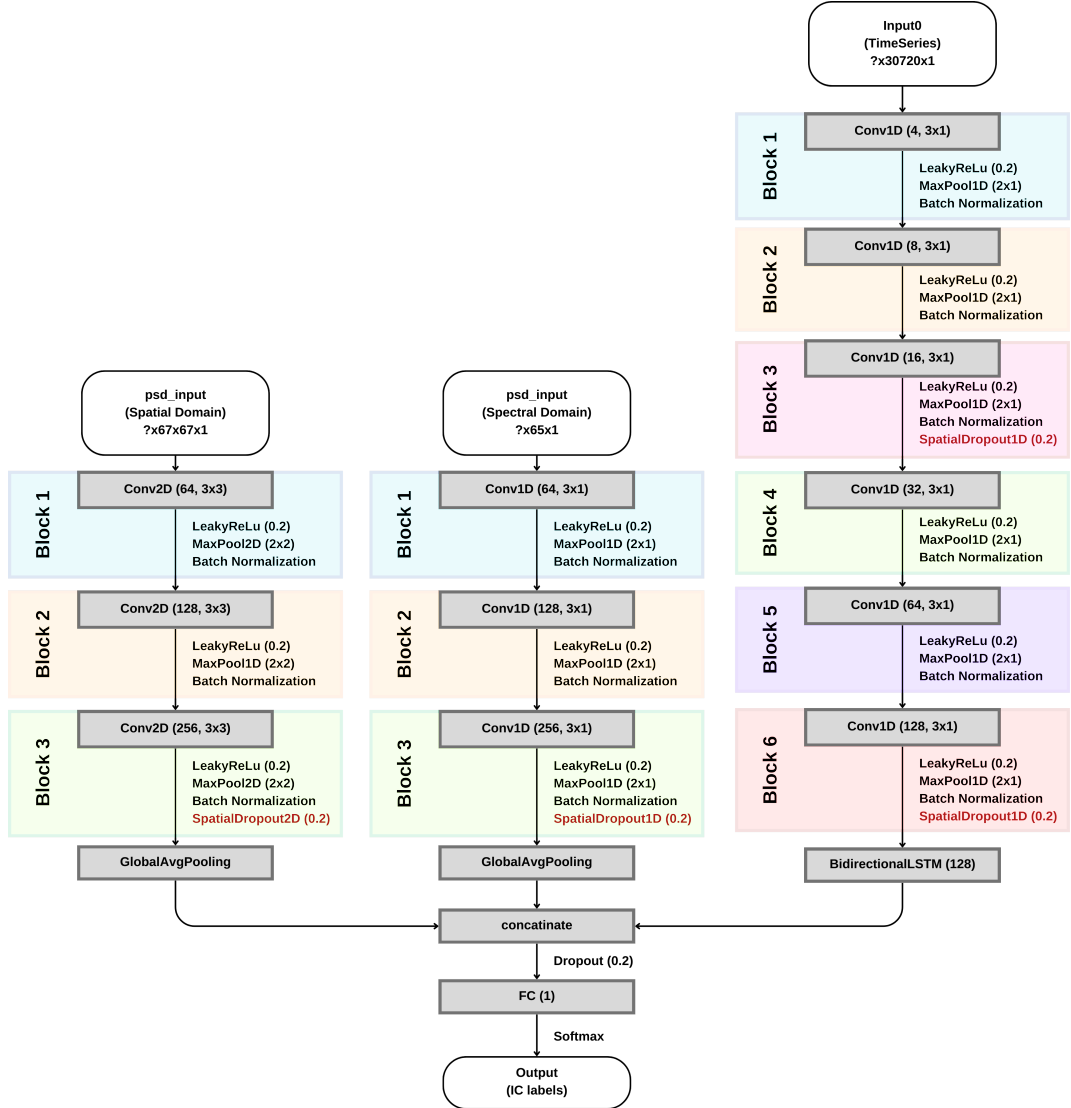


Figure 3.20: Independent component label model architecture

1. The leaky ReLu function has been used to handle the vanishing gradient problem. Six max-pooling layers with 2×1 as the kernel and stride as one have been used to downsample the layers. Dropout layers and spatial dropout layers have been used to reduce overfitting. A BiLSTM layer has been used at the end of the encoder head to extract temporal features in both directions. The size has been set to match the outputs of the other two networks. Additionally, batch normalization layers were added to stabilize the learning process.

In the spectral domain network, as in the temporal network, three convolutional layers (from 64-256 filters) are used to extract frequency domain features. Also, leaky ReLu activation, 1D max pooling, and batch normalization have been used in the DNN. A global average pooling layer has been added at the end to reduce each feature vector to a single value. A similar network with 2D convolution layers has been used in the spatial convolution network. The fully connected layer does the final classification after concatenating the above-mentioned

DNNs.

To train the dataset the 10-minute independent components were broken into 2-minute epochs. To train the model a batch size of 32 was used, and binary cross entropy as the loss function along with ADAM optimizer.

Scaling Function

To scale the input to any time interval greater than 2 minutes, the signal is broken into a number of epochs where,

$$a = \left\lceil \frac{\text{Total length of the input}}{\text{Length of a single epoch}} \right\rceil \quad (3.12)$$

The overlaps are divided equally between the epochs. To reconstruct the signal with overlaps, overlapped area is averaged by the number of overlaps.

3.3.3 Graphical User Interface

To ensure efficient use by healthcare professionals, the GUI was developed with a focus on functionality. Figure 3.21 depicts the typical workflow a medical professional can expect when interacting with the software.

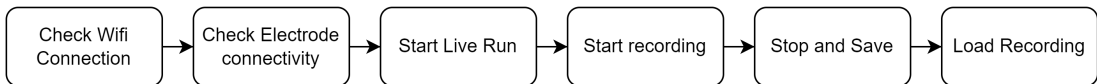


Figure 3.21: Expected flow when using the GUI

Check Connectivity

Initially, it is necessary to check the connectivity of the electrodes before capturing data. For this, a separate window shows the connectivity of separate electrodes. EEG from different channels are shown in each graph. The data from the graphs can be interpreted as follows.

- All channels red → Cz or the ground electrode is not in proper contact
- A single channel red → The particular electrode is not in contact
- All channels green → Possible to start capturing data

Figure 3.22 shows an instance where the O1 electrode is not in proper contact.

Movement Detection

The data from IMU sensors can be viewed using the IMU window. Figure 3.23 shows an instance where a head movement has occurred. Movements are detected by thresholding the variance of the data from the IMU sensor.

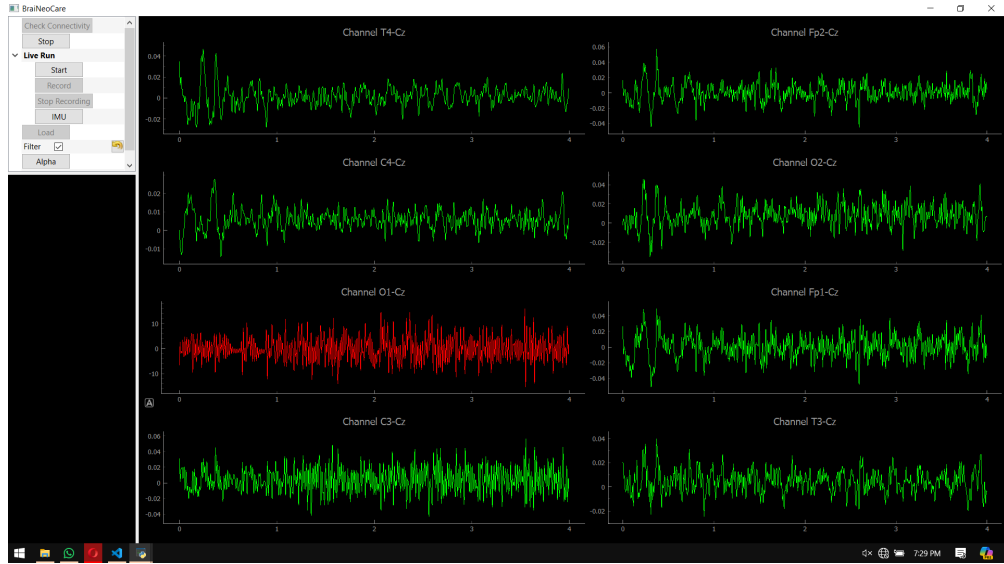


Figure 3.22: Check connectivity interface with O1 channel not in contact

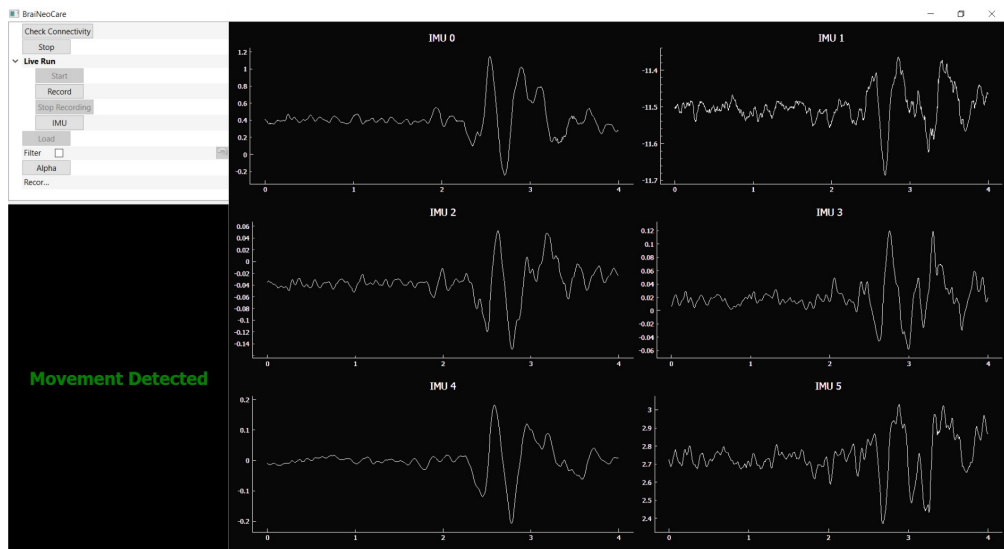


Figure 3.23: IMU data interface with movement detection

Live Run and Seizure Detection

After proper electrode connectivity has been ensured, the user can start a live run. The live run shows the common 12-channel electrode configuration used in hospital settings. During the live run, the user can start recording the data using the Record button. This is indicated in the GUI as shown in fig. 3.24.

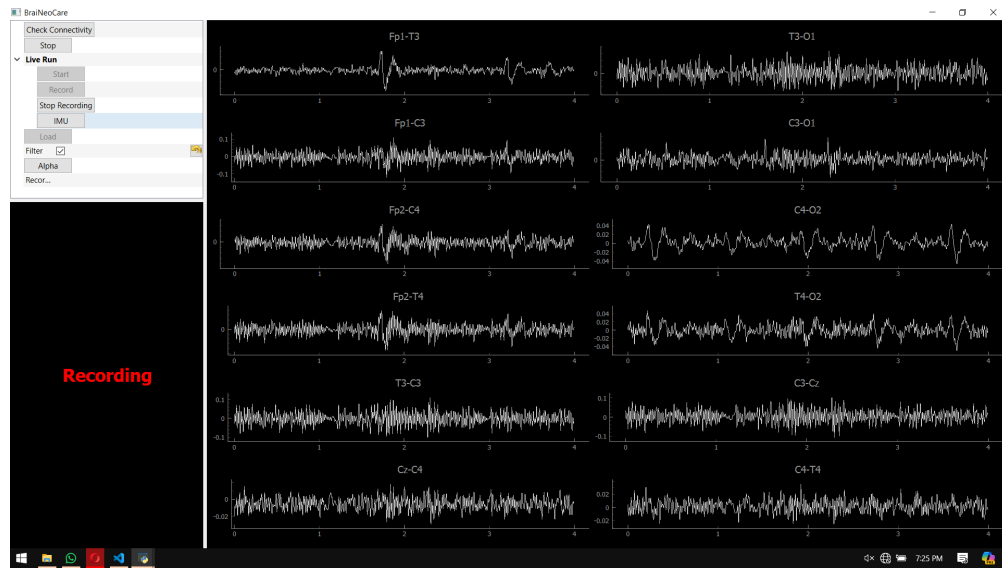


Figure 3.24: Live run while data are recorded

If a seizure is detected during the live run, all graphs turn red, indicating the detection of a seizure. The user can decide to turn on/off the digital filters (50 Hz Notch, 2-90 Hz Bandpass) to get a clean signal. Further, the GUI allows easy zooming and panning capabilities for the user.

Save Load Functions

After the data is recorded the user can load the data using the Load Data button. The user will be allowed to select the necessary file where the data was stored.

After loading data, the automatic artifact removal algorithm and the interpretability algorithms will run. The GUI shows the separate seizure-detected areas using the interpretability algorithm and the clean signal with the removed artifacts.

Game using Alpha Waves

In order to show the functionality of the device, we have added a small game that works using alpha waves captured in the visual cortex of the brain.

The alpha wave frequencies (8-13 Hz) are bandpass filtered and the variance of the signal is thresholded to identify the alpha waves. Alpha waves are easily generated in the visual cortex of the brain when the eyes are closed. A small game is created using pygame to make an apple float after alpha waves are detected.

3.4 Clinical Trials

EEG signals have an incredibly low amplitude ($10 - 100 \mu\text{V}$). They are 100 to 1000 times weaker than other biosignals in the body, making them susceptible to contamination by various noises. Therefore, ensuring high-quality EEG recordings is crucial.

Our initial quality assessment involved recording alpha waves from group members. However, to truly validate our system, we needed to compare it to a commercial device and test its functionality during seizures.

Testing on patients experiencing seizures presented an ethical challenge. Therefore, we wanted to test the system with one of the mildest forms of seizures - absence seizures. However, They primarily affect children and are uncommon. To address these issues, we collaborated with Lady Ridgeway Hospital for Children and obtained ethical approval from the University of Moratuwa Ethical Research Committee (Ethics Declaration Number: ERN/2024/001). All tests adhered to strict ethical guidelines, and informed consent was acquired from participants' parents before testing began.

To directly compare recordings, we employed both the hospital's wet electrode system (Nihon Kohden JE-921 - Hereafter referred to as wet electrode system) and our dry electrode system simultaneously. Electrodes were positioned as close as possible in similar locations to minimize any influence on the recordings.



Figure 3.25: Clinical testing on an absence seizure patient with both the commercial wet electrode system and our dry electrode system

Chapter 4

Results and Discussion

4.1 Signal Quality

Correlation

Visual analysis of raw EEG signals revealed a strong similarity between our dry electrode-based recordings and the wet electrode system fig. 4.1.

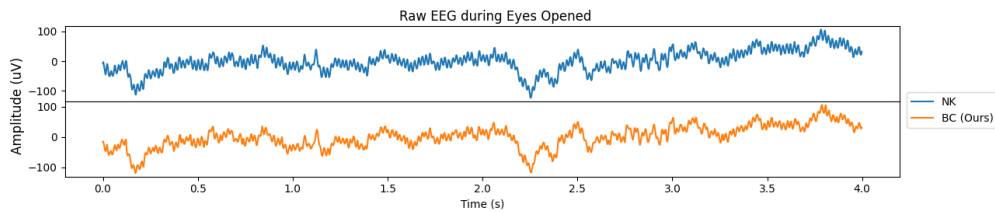


Figure 4.1: EEG during eyes open

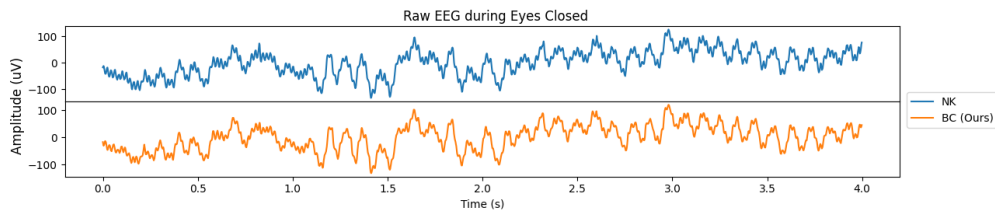


Figure 4.2: EEG during eyes closed

However, to analyze quantitatively, we used a 2-30 Hz filter on the recordings and calculated the correlation between the wet electrode and dry electrode system. The details regarding the samples used for this calculation are shown in table 4.1.

The average correlation across multiple samples and channels is presented in Figure Figure 4.4. Notably, the correlation values tend to increase during alpha wave generation and rise further during seizures. This observation aligns with the inherent nature of EEG signals – higher amplitude activity leads to stronger correlations.

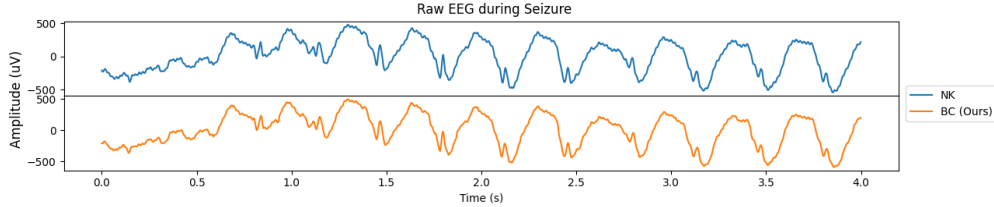


Figure 4.3: EEG during seizure

Table 4.1: Dataset used to calculate signal quality

State	Number of Samples	Total Length (s)
Eyes Opened	7	41
Eyes Closed	6	83
Seizure	4	58.06

Signal to Noise Ratio (SNR)

To calculate the SNR, we must first examine the Frequency spectrum of the obtained signals. The frequency spectrum during various states of the raw EEG compared in the two devices are shown in fig. 4.5.

Looking at the FFT, we can see that a higher 50 Hz powerline noise can be observed in the recordings from the wet electrode system.

Calculating the signal-to-noise ratio (SNR) in EEG data is complex due to the difficulty of isolating pure noise. Previous studies have estimated SNR by comparing the power of the alpha band to the 2-30 Hz bandpassed EEG signal. However, since EEG signals are not limited to the 2-30 Hz range, this method has limitations.

To address this, we explored two alternative approaches for SNR estimation:

1. **Powerline frequency as the noise signal:** We considered the 50 Hz powerline noise as the primary noise component within the 2-90 Hz bandpass signal.
2. **Alpha wave as true signal:** We treated the alpha wave as the true signal of interest within the 2-90 Hz bandpass signal, with the remaining components considered noise.

The results of these SNR calculations are presented in fig. 4.6. Notably, our device consistently achieved higher or comparable SNR values across all three methods compared to the wet electrode system.

Noise During Movements

Dry-electrode EEG devices are known to be sensitive to movement artifacts. While our device exhibited minimal signal variations during small movements such as breathing, larger noise disruptions were observed when the user fell asleep and experienced head movements. This is likely due to the lightly attached electrodes to ensure user comfort.

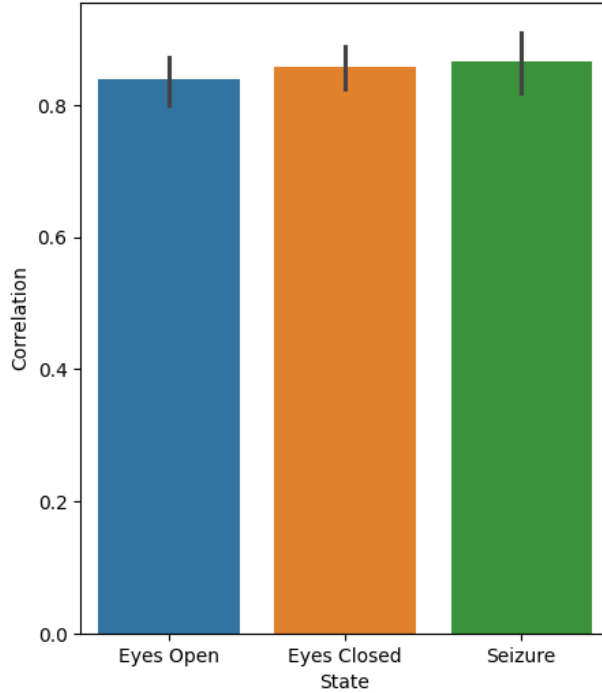


Figure 4.4: Correlation between data recorded from wet electrode and dry electrode system

Interestingly, the O1/O2 electrodes (which presumably made good contact) displayed movement noise levels comparable to wet electrodes. This suggests that the core technology functions well. However, other electrodes with looser contact experienced brief periods of signal disruption during movement. To mitigate this, future iterations could explore improvements to the electrode design, such as spring-loaded mechanisms or flexible materials, to achieve a better balance between user comfort and signal stability.

4.2 Specifications of the Device

The main specifications of the device are shown in the following table 4.2.

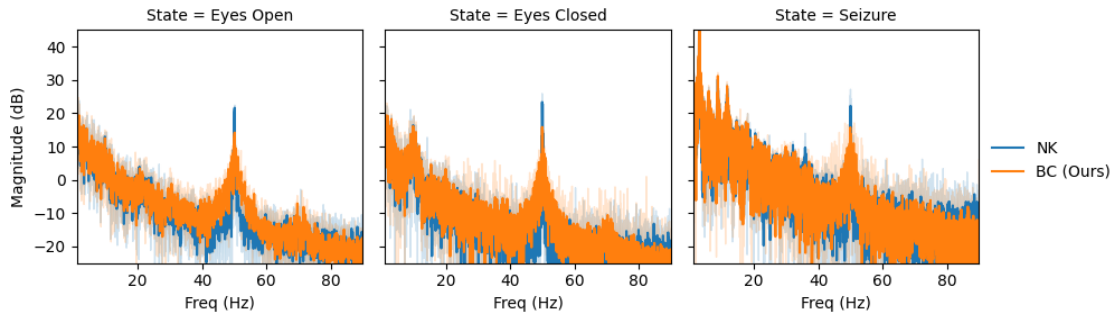


Figure 4.5: FFT of recorded data during various states

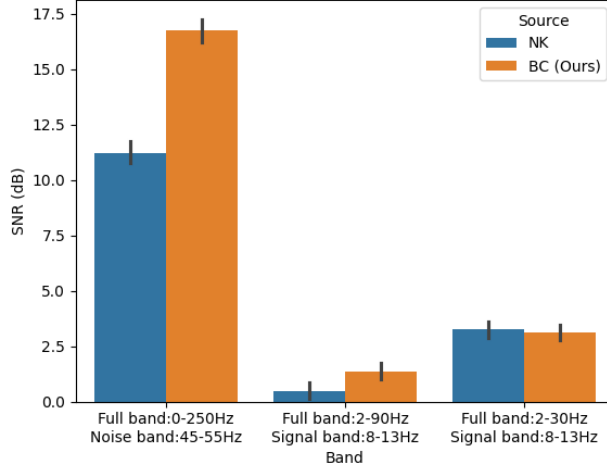


Figure 4.6: SNR of recorded data

Table 4.2: Device specifications

Number of channels	8
Electrode montage	Reduced 10-20 layout
Safety	USB Isolator, Body Safety Resistor, ESD Protection
Input bias current	0.2 pA
CMRR	>110 dB
Highpass filter	0.1 Hz
Lowpass filter	120 Hz
Sampling frequency	250 Hz
Battery capacity	1200 mAh
Device current draw	300 mA
Usable time	4 hours

4.3 Machine Learning

This section is dedicated to talking about the output results from the deep learning model. As we developed several deep learning models throughout this research, we are going to discuss the results of all those models. For all the cases we divided the data set, 80% for the training dataset and 20% for the test dataset. Accuracy metric was used as a common evaluation method for all these methods, but sometimes we used other evaluation matrices such as AUC, precision, recall, and kappa. For the first model which is similar to the ResNet50 model, we could obtain around 67% accuracy and the next fully CNN-based tiny network showed a better accuracy of 82.38% and AUC of 85.61%. When it comes to our proposed final model, we trained and evaluated it using the above-mentioned 80%-20% datasets and we performed 10-fold cross-validation as well. For the first method, we obtained 91.56%, 94.42%, 83.22%, 88.61%, and 0.8 for accuracy, AUC, recall, precision, and kappa respectively. For the cross-validation, we obtained mean values of 89.02%, 91.46%, 82.84%, 94.23%, and 0.89 for accuracy, AUC, recall, precision, and kappa respectively.

Apart from these numbers, our model explains the output. We take the derivative of the model output with respect to the weights of the last GAT layer to interpret the model output for a given input EEG epoch. This is similar to Grad-CAM[39] but different. In this way we explain which channels and time ranges were given high priority to give the output. Based on this we can understand if the model correctly detects a seizure. As well as our model also has the capability of detecting seizures in real-time on a CPU and explaining the result within 70ms. Figure 4.7 shows a 12s EEG epoch with its heatmap to explain the model output.

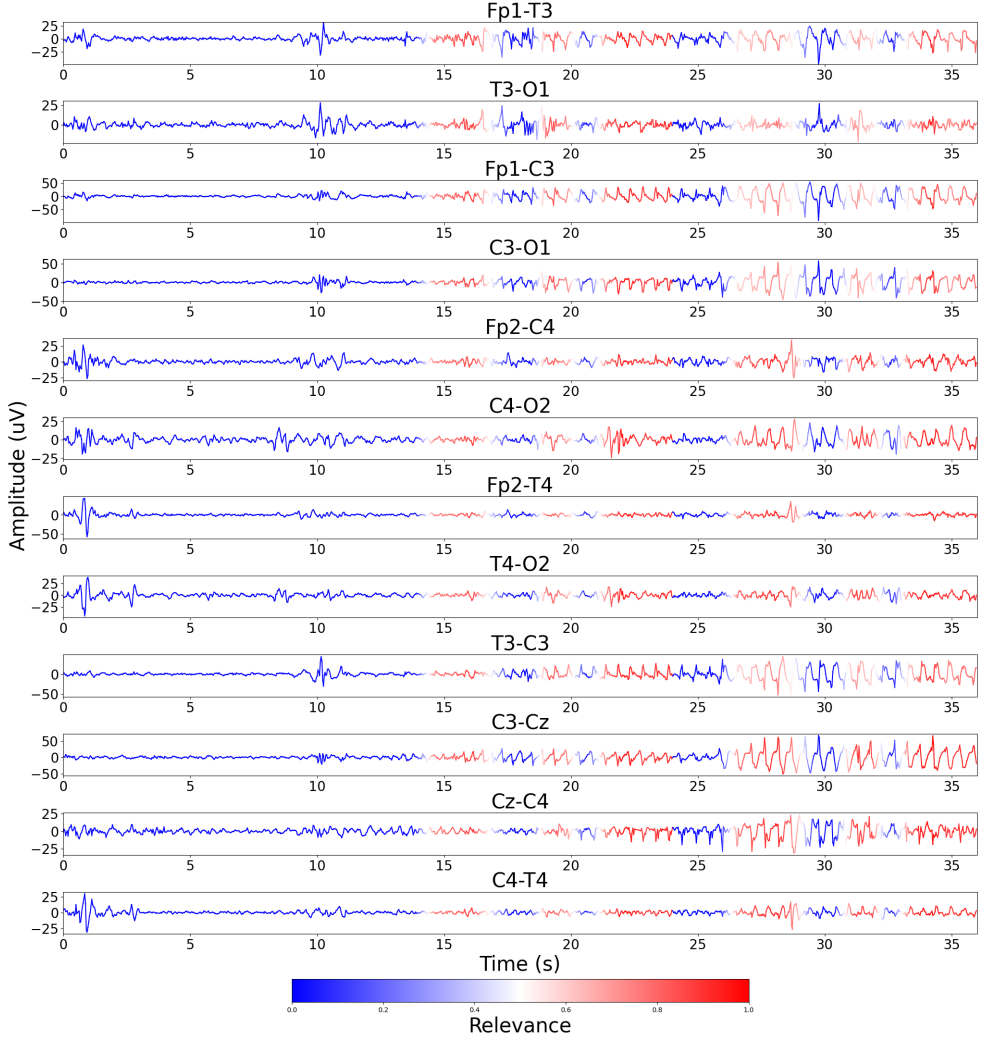


Figure 4.7: Visualization of the epoch with its heatmap. Dark blue represents the zero relevance while dark red represents the highest relevance. The relevance is given as probability. This is a seizure epoch and the model detected this as a seizure epoch.

Comparing the results of previously published models with our proposed method is inequitable as all the previously published methods process 18 EEG channels which are obtained from a totally different electrode montage. But in Table 4.3, we have given a full comparison between previous methods and our method. To verify if our model performs

Table 4.3: Model performance comparison. CV- Cross Validation

Number of EEG channels	Method	Accuracy	AUC		Recall	Precision	Kappa
		mean± std	Median (IQR)	Mean±std			
18	MSC-GCNN[69]	-	99.1 (96.8,99.6)	94.7±10.9	96.71	-	0.8
	PLV-GCNN[69]	-	99.0 (95.2,99.7)	94.1±10.5	95.3	-	0.79
	SD-GCNN[69]	-	97.3 (86.3,99.6)	90.09±13.5	96.68	-	0.71
	ST-GAT(FL)[37]	-	99.3 (96.4,99.5)	96.6±8.9	98	-	0.88
12 10-fold CV	ST-GAT(FL)	80.29±9.48	83.98 (77.8,90.9)	83.15±8.85	39.98	94.91	0.43
	Our method	89.02±2.91	91.84 (88.57,95.21)	91.46±4.36	82.84	94.23	0.89
12 (80%-20%)	ST-GAT(FL)	88.8	91.71		66.89	95.17	0.71
	Our method	91.56	94.42		83.22	88.61	0.80

better than the state-of-the-art model, we trained and evaluated the state-of-the-art model for 12 channels and it produced very bad results compared to ours as reported in Table 4.3. According to these results, we can state that our model is a new state-of-the-art model for neonatal seizure detection with 12 channels.

4.4 Signal Processing

Results of the trained model and comparison with the old model and ICAlabel model

The independent component label model, trained on the EPIC dataset as detailed in the methodology section focusing on signal processing, demonstrates its performance in Table 4.4. Two variations of the model denoted as IC-label_{bc}-our model and IC-label_{en}-publication, are compared based on their accuracy, area under the curve (AUC), F1-score, precision, and recall across different classes. For the custom-trained model, an overall accuracy of 91.96% with an AUC of 91.85% is achieved, showcasing a slightly better performance. Class-wise analysis reveals a high F1-score of 92% for non-artifactual instances, indicating the model's proficiency in distinguishing non-artifactual signals. However, the model's precision and recall for the artifactual class are slightly lower, at 88% and 91%, respectively. On the other hand, the publication's model achieves an accuracy of 90.09% and an AUC of 90.90%, with similar trends observed in class-wise evaluation.

Table 4.4: Model performance comparison of the IC label model

Model	Class	Accuracy	AUC	F1-score	Precision	Recall
IC-label _{bc} (our)		91.96%	91.85%	92%	-	-
	0 (Artifactual)	-	-	89%	88%	91%
	1 (Non-Artifactual)	-	-	93%	95%	92%
IC-label _{en} (publication)		90.09%	90.90%	90%	-	-
	0 (Artifactual)	-	-	88%	82%	94%
	1 (Non-Artifactual)	-	-	92%	96%	88%

The model is unable to scale to the given data input size, however, a separate algorithm was made to scale down the input to 2-minute epochs so that the process allows for scaling of the input data, as mentioned in the methodology.

Results Obtained from the Lady Ridgeway Hospital

The inputs to the machine learning model using the data obtained at LRH are as given below in figure 4.8 and figure 4.9.

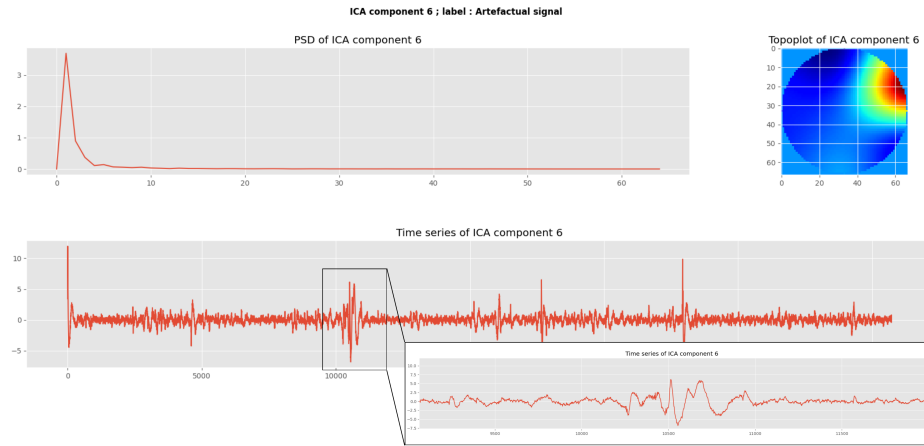


Figure 4.8: Independent component classified as artifact

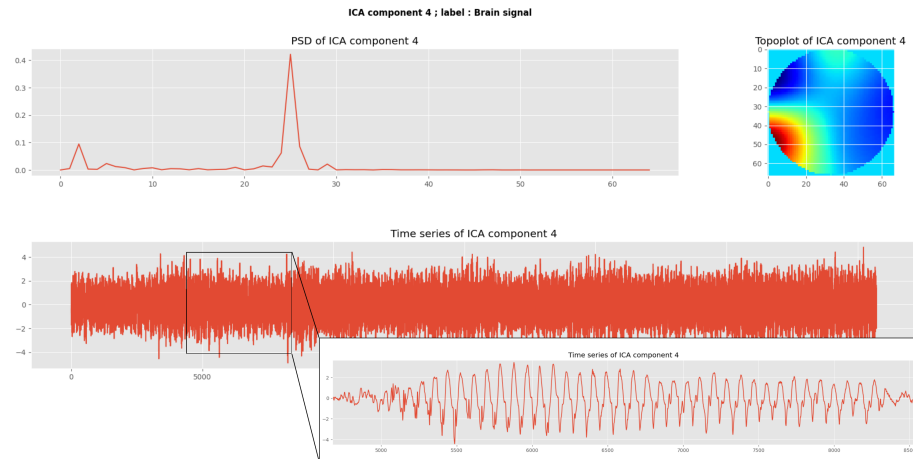


Figure 4.9: Independent component classified as brain waves from a seizure onset

In these images, the IC component, clearly visible as an eye artifact in the time-series plot and the topological plot by indicating relevance to the Fp1 and Fp2 electrodes, is labelled as an artifact by the IC label model. In the following figure, the IC extracted using a seizure timeframe has also been labelled as a brain signal by the IC label model.

The figure in 4.10 indicates one such artifact correctly removed from the algorithm from the Fp1 and Fp2 electrodes. The following figure indicates a seizure pattern not identified as an artifact by the algorithm. It is noticeable that even though the seizure pattern and

the eye artifact had similar frequency and time-series components, the IC label model could correctly differentiate between them.

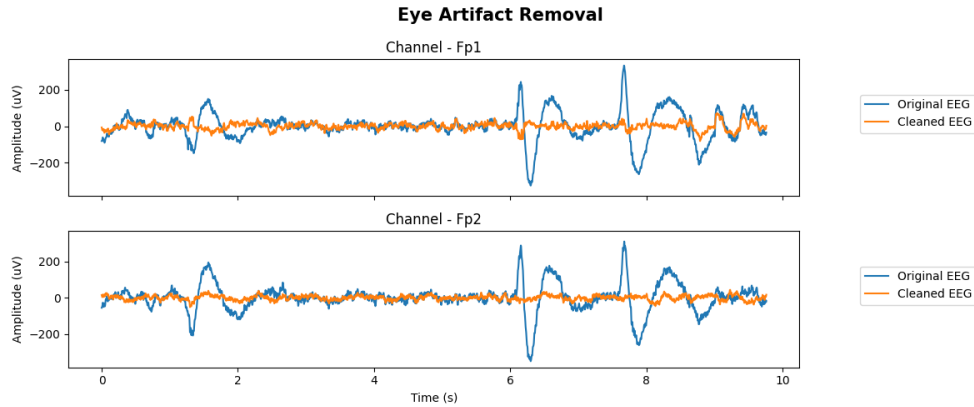


Figure 4.10: Independent component removing eye artifacts from the data obtained at Lady Ridgeway Hospital

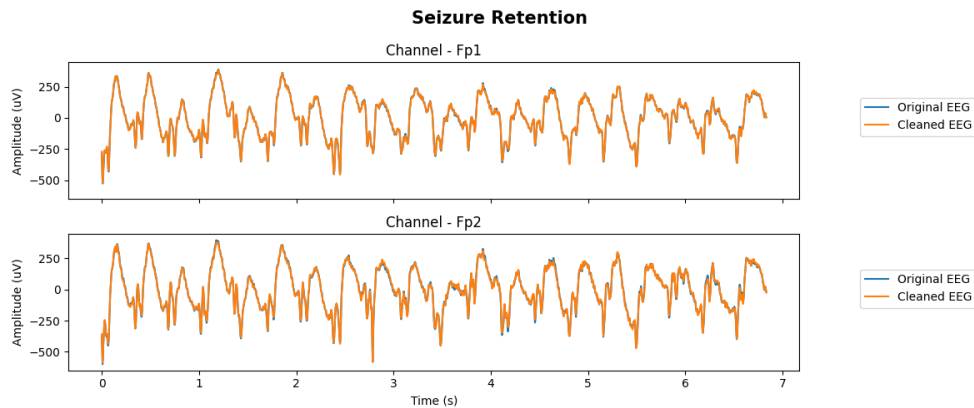


Figure 4.11: Independent component retaining seizures from the data obtained at Lady Ridgeway Hospital

Two other methods that were tested earlier, are indicated as below.

In the figures depicted by figure 4.12, 4.13, 4.14, and 4.15 it is clearly visible that the mne's ICA labelling method performs poorly on the seizure data while the ATAR algorithm (based on packet wavelet decomposition) performs poorly when differentiating between artifacts and seizure waves. This is due to the fact that DNN is able to extract non-linear features from the data sets during the model training process. Therefore it can be concluded that DNNs perform better than classical wavelet decomposition methods. Since the EPIC dataset consists of seizure data, our model outperforms the current state-to-art model ICAlabel.

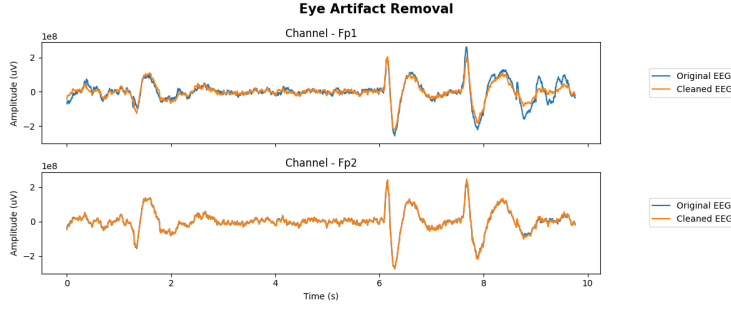


Figure 4.12: Independent component failing to remove eye artifacts from the data obtained at Lady Ridgeway Hospital - using mne ICAlabeling method



Figure 4.13: Independent component retaining seizures from the data obtained at Lady Ridgeway Hospital - using mne ICAlabeling method

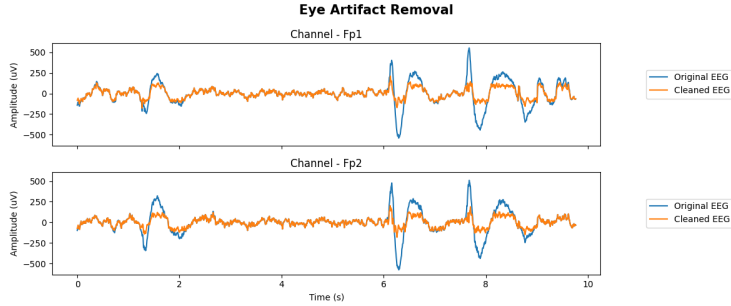


Figure 4.14: Independent component removing eye artifacts from the data obtained at Lady Ridgeway Hospital - using ATAR method



Figure 4.15: Independent component removing seizures from the data obtained at Lady Ridgeway Hospital - using ATAR method

4.5 Device User Feedback

Device Comfortability Test

The device was only tested for an 8-year-old child in a clinical setting along with the information sheets and consent forms. After the test was performed, the patient along with the parent was advised to fill in the questionnaire regarding how much the patient was comfortable with using our device compared to the wet electrode system used at the hospital. There we got feedback from the patient that he was comfortable while wearing the device and he will be happy to wear our device again for an EEG signal-capturing test.

A device user feedback test was done at the Biomedical Laboratory at the Department of Electronic and Telecommunication Engineering at the University of Moratuwa on the 19th of April. The device was worn on 20 volunteers, each person for 5 minutes and a connectivity check was done to confirm the electrodes were in contact with the head well. The time taken to wear the device was also measured. Later to the same volunteer, gel-based wet electrodes were fixed on the head using a similar procedure in the hospital setting. Then a Google form was filled out by the volunteer regarding the time taken to wear the device and comfortability during and after wearing the device. The summary of the results is given below.

Average time to wear the device = 67.8s

Rate of preference for the device we developed for EEG signal capturing compared to the conventional method = 100%

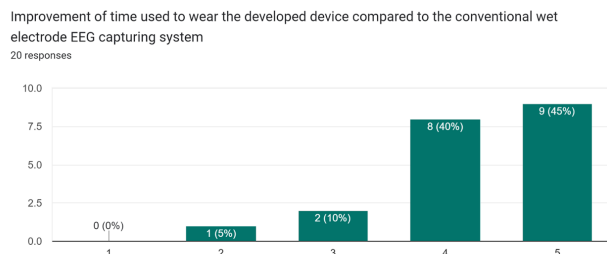


Figure 4.16: Improvement of time compared to the conventional device

The above test results imply that the system we developed has a significant improvement in assemble time compared to the conventional wet-electrode-based system and users are much more comfortable during and after wearing the developed device for some time.

Electrode Mark

Due to the spike shape of the dry electrode, we are using in this device, it causes a mark with the pressure applied for a long time to the forehead and other areas where the electrode is in contact with the skin. Marks in the forehead area are comparatively more visible due to the lack of hair in that region. With time, the mark disappears. The amount of visibility of the electrode mark with time is shown in the image below

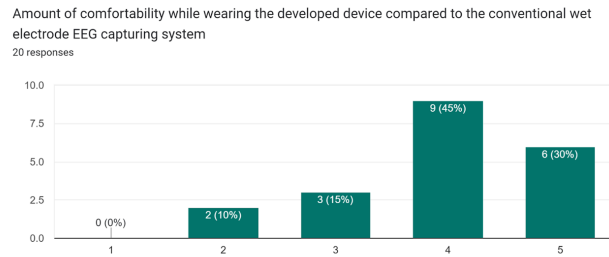


Figure 4.17: Amount of comfortability while wearing the device

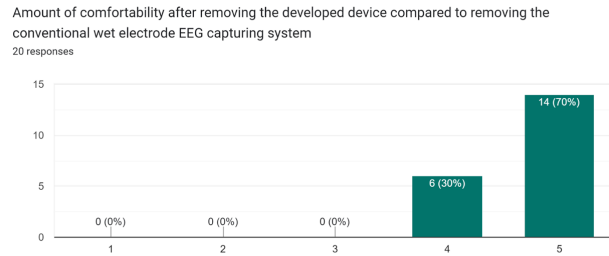


Figure 4.18: Amount of comfortability after removing the device

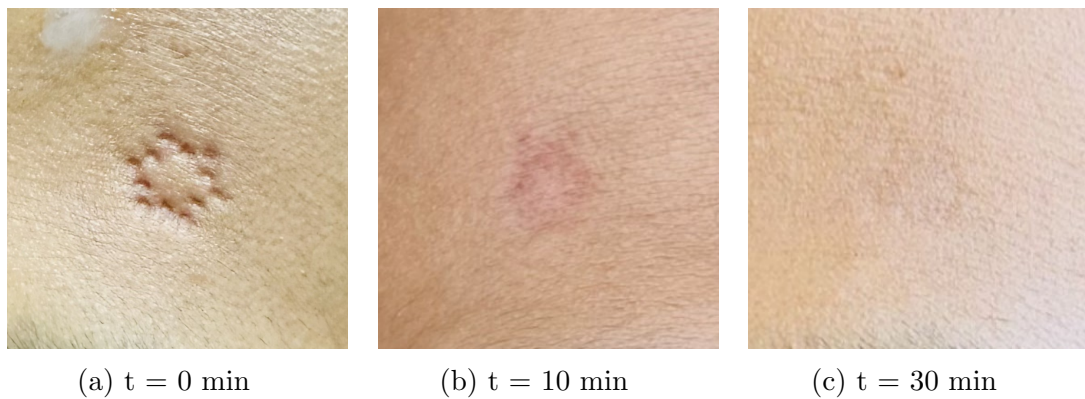


Figure 4.19: Electrode mark visibility with time

Chapter 5

Conclusion

In conclusion, our project successfully addresses the significant challenge of identifying neonatal seizures, mainly detectable through EEGs. The limitations of traditional wet electrode EEG systems, including their cumbersome nature and attachment difficulty, led us to develop an innovative device. Our device has overcome the high noise levels associated with conventional dry electrode headsets and surpassed the signal-to-noise ratio (SNR) of clinically used wet electrode-based EEG devices during trials. A standout feature of our device is its capability for real-time wireless data transmission, coupled with a machine learning algorithm proficient in accurately identifying seizures. This algorithm outperformed the state-of-the-art models and incorporated explainability into the entire pipeline, enhancing understanding and trust in its findings. Moreover, our device includes an offline artifact removal algorithm that effectively distinguishes between artifacts and seizures, ensuring reliable data analysis.

As future work, we aim to refine the device's ergonomics, implement spring-loaded or flexible electrodes for ease of use, begin commercialization, and enhance the model's performance through real-time artifact removal. Later with the ethical clearance the device can be tested on neonates. This comprehensive approach not only showcases the technological advancements of our device but also sets a new standard for the future of neonatal seizure detection and monitoring.

References

- [1] H. Tekgul, D. Blaise, K. Gauvreau, and A. Bergin, “Electroencephalography in neonatal seizures: Comparison of a reduced and a full 10/20 montage,” *Pediatric neurology*, vol. 32, pp. 155–61, 04 2005.
- [2] C. Krawiec and M. R. Muzio, “Neonatal seizure,” in *StatPearls [Internet]*, StatPearls Publishing, 2023.
- [3] J. Wanigasinghe, R. Kapurubandara, C. Arambepola, S. Sri Ranganathan, and J. Philips, “Incidence of neonatal seizures in babies born in two premier maternity hospitals within colombo city,” *Association of Sri Lankan Neurologists 11th Annual Academic Sessions 2017*, pp. 43,44, 2017.
- [4] M. Teplan *et al.*, “Fundamentals of eeg measurement,” *Measurement science review*, vol. 2, no. 2, pp. 1–11, 2002.
- [5] A. G. Sandoval Karamian and C. J. Wusthoff, “Current and future uses of continuous eeg in the nicu,” *Frontiers in Pediatrics*, vol. 9, 2021.
- [6] H. Chen, Z. Wang, C. Lu, F. Shu, C. Chen, L. Wang, and W. Chen, “Neonatal seizure detection using a wearable multi-sensor system,” *Bioengineering*, vol. 10, no. 6, 2023.
- [7] S.-K. Lin, Istiqomah, L.-C. Wang, C.-Y. Lin, and H. Chiueh, “An ultra-low power smart headband for real-time epileptic seizure detection,” *IEEE Journal of Translational Engineering in Health and Medicine*, vol. 6, pp. 1–10, 2018.
- [8] A. Omurtag, S. G. A. Baki, G. Chari, R. Q. Cracco, S. Zehtabchi, A. A. Fenton, and A. C. Grant, “Technical and clinical analysis of microeeg: a miniature wireless eeg device designed to record high-quality eeg in the emergency department,” *International Journal of Emergency Medicine*, vol. 5, pp. 1–10, 2012.
- [9] T. Grummett, R. Leibbrandt, T. Lewis, D. DeLosAngeles, D. Powers, J. Willoughby, K. Pope, and S. Fitzgibbon, “Measurement of neural signals from inexpensive, wireless and dry eeg systems,” *Physiological measurement*, vol. 36, no. 7, p. 1469, 2015.
- [10] TMSI, “Types of eeg electrodes: Gel, water, and dry.” <https://info.tmsi.com/blog/types-of-eeg-electrodes>.
- [11] G. Di Flumeri, P. Aricò, G. Borghini, N. Sciaraffa, A. Di Florio, and F. Babiloni, “The dry revolution: Evaluation of three different eeg dry electrode types in terms of signal

- spectral features, mental states classification and usability,” *Sensors*, vol. 19, no. 6, p. 1365, 2019.
- [12] L. Popović-Maneski, M. Ivanović, V. Atanasoski, M. Miletić, S. Zdolšek, B. Bojović, and L. Hadžievski, “Properties of different types of dry electrodes for wearable smart monitoring devices,” *Biomed Tech (Berl)*, vol. 65, no. 4, pp. 405–415, 2020.
 - [13] A. J. Casson, M. Abdulaal, M. Dulabh, S. Kohli, S. Krachunov, and E. Trimble, “Electroencephalogram,” in *Seamless Healthcare Monitoring*, ch. 2, p. 45–81, Springer Cham, 1st ed., 2017.
 - [14] A. Pourahmad and A. Mahnam, “Evaluation of a low-cost and low-noise active dry electrode for long-term biopotential recording,” *J Med Signals Sens*, vol. 6, pp. 197–202, Oct-Dec 2016.
 - [15] Y. Jiang, O. Samuel, X. Liu, X. Wang, O. Idowu, P. Li, F. Chen, M. Zhu, Y. Geng, S. Chen, and P. Li, “Effective biopotential signal acquisition: Comparison of different shielded drive technologies,” *Applied Sciences*, vol. 8, 02 2018.
 - [16] M. Guermandi, E. F. Scarselli, and R. Guerreri, “A driving right leg circuit (dgrl) for improved common mode rejection in bio-potential acquisition systems,” *IEEE transactions on biomedical circuits and systems*, vol. 10, pp. 507–517, 2015.
 - [17] Y. Li, H. Pan, and Q. Song, “Ads1299-based array surface electromyography signal acquisition system,” in *Journal of Physics: Conference Series*, vol. 2383, p. 012054, IOP Publishing, 2022.
 - [18] M. B. Pires, J. J. A. M. Junior, and S. L. Stevan Jr, “Development of an 8 channel semg wireless device based on ads1299 with virtual instrumentation,” *arXiv preprint arXiv:1808.03711*, 2018.
 - [19] G. D. Gargiulo, P. Bifulco, M. Cesarelli, A. McEwan, A. Nikpour, C. Jin, U. Gunawardana, N. Sreenivasan, A. Wabnitz, and T. J. Hamilton, “Fully open-access passive dry electrodes bioadc: Open-electroencephalography (eeg) re-invented,” *Sensors*, vol. 19, no. 4, p. 772, 2019.
 - [20] L. Toresano, S. K. Wijaya, P. Prawito, A. Sudarmaji, and C. Badri, “Data acquisition system of 16-channel eeg based on atsam3x8e arm cortex-m3 32-bit microcontroller and ads1299,” in *AIP Conference Proceedings*, vol. 1862, AIP Publishing, 2017.
 - [21] U. Rashid, I. K. Niazi, N. Signal, and D. Taylor, “An eeg experimental study evaluating the performance of texas instruments ads1299,” *Sensors*, vol. 18, no. 11, p. 3721, 2018.
 - [22] Z. Ibrahim, G. Chari, S. Abdel Baki, V. Bronshtein, M. Kim, J. Weedon, J. Cracco, and J. Aranda, “Wireless multichannel electroencephalography in the newborn,” *J Neonatal Perinatal Med*, vol. 9, no. 4, pp. 341–348, 2016.
 - [23] E. Senechal, D. Radeschi, L. Tao, S. Lv, E. Jeanne, R. Kearney, W. Shalish, and G. Sant Anna, “The use of wireless sensors in the neonatal intensive care unit: a study protocol,” *PeerJ*, vol. 11, p. e15578, Jun 2023.

- [24] Food and D. Administration, “510(k) summary for sibel inc.’s anne one,” Sep 2021.
- [25] I. Ahmad, X. Wang, M. Zhu, C. Wang, Y. Pi, J. A. Khan, S. Khan, O. W. Samuel, S. Chen, and G. Li, “Eeg-based epileptic seizure detection via machine/deep learning approaches: A systematic review,” *Computational Intelligence and Neuroscience*, 2022.
- [26] R. San-Segundo, M. Gil-Martín, L. F. D’Haro-Enríquez, and J. M. Pardo, “Classification of epileptic eeg recordings using signal transforms and convolutional neural networks,” *Computers in Biology and Medicine*, vol. 109, pp. 148–158, 2019.
- [27] A. Temko, E. Thomas, W. Marnane, G. Lightbody, and G. Boylan, “Eeg-based neonatal seizure detection with support vector machines,” *Clinical Neurophysiology*, 2011.
- [28] Z. Li, Y. Fang, Y. Li, K. Ren, Y. Wang, X. Luo, J. Duan, C. Huang, D. Li, and L. Qiu, “Protecting the future: Neonatal seizure detection with spatial-temporal modeling,” *IEEE International Conference on Systems, Man, and Cybernetics*, July 2023.
- [29] Z. Liu, A. Alavi, M. Li, and X. Zhang, “Self-supervised contrastive learning for medical time series: A systematic review,” *Sensors for Physiological Parameters Measurement, Sensors*, vol. 23, 4221, 2023.
- [30] S. Das, P. Pandey, and K. P. Miyapuram, “Improving self-supervised pretraining models for epileptic seizure detection from eeg data,” *Electrical Engineering and Systems Science*, June 2022.
- [31] M. L. Giudice, N. Mammone, C. Ieracitano, M. Campolo, A. R. Bruna, V. Tomaselli, and F. C. Morabito, “Visual explanations of deep convolutional neural network for eye blinks detection in eeg-based bci applications,” in *2022 International Joint Conference on Neural Networks (IJCNN)*, pp. 01–08, IEEE, 2022.
- [32] Q. H. Cao, T. T. H. Nguyen, V. T. K. Nguyen, and X. P. Nguyen, “A novel explainable artificial intelligence model in image classification problem,” *arXiv preprint arXiv:2307.04137*, 2023.
- [33] A. Temko, E. Thomas, W. Marnane, G. Lightbody, and G. Boylan, “Eeg-based neonatal seizure detection with support vector machines,” *Clinical Neurophysiology*, vol. 122, no. 3, pp. 464–473, 2011.
- [34] P. Thodoroff, J. Pineau, and A. Lim, “Learning robust features using deep learning for automatic seizure detection,” in *Proceedings of the 1st Machine Learning for Healthcare Conference* (F. Doshi-Velez, J. Fackler, D. Kale, B. Wallace, and J. Wiens, eds.), vol. 56 of *Proceedings of Machine Learning Research*, (Northeastern University, Boston, MA, USA), pp. 178–190, PMLR, 18–19 Aug 2016.
- [35] M. S. Hossain, S. Amin, M. Alsulaiman, and G. Muhammad, “Applying deep learning for epilepsy seizure detection and brain mapping visualization,” *ACM Transactions on Multimedia Computing, Communications, and Applications*, vol. 15, pp. 1–17, 02 2019.
- [36] Z. Li, Y. Fang, Y. Li, K. Ren, Y. Wang, X. Luo, J. Duan, C. Huang, D. Li, and L. Qiu, “Protecting the future: Neonatal seizure detection with spatial-temporal modeling,” 2023.

- [37] K. Raeisi, M. Khazaei, G. Tamburro, P. Croce, S. Comani, and F. Zappasodi, “A class-imbalance aware and explainable spatio-temporal graph attention network for neonatal seizure detection,” *International Journal of Neural Systems*, vol. 33, 06 2023.
- [38] M. L. Giudice, N. Mammone, C. Ieracitano, M. Campolo, A. R. Bruna, V. Tomaselli, and F. C. Morabito, “Visual explanations of deep convolutional neural network for eye blinks detection in eeg-based bci applications,” in *2022 International Joint Conference on Neural Networks (IJCNN)*, pp. 01–08, 2022.
- [39] R. R. Selvaraju, M. Cogswell, A. Das, R. Vedantam, D. Parikh, and D. Batra, “Grad-cam: Visual explanations from deep networks via gradient-based localization,” in *2017 IEEE International Conference on Computer Vision (ICCV)*, pp. 618–626, 2017.
- [40] S. Das, P. Pandey, and K. P. Miyapuram, “Improving self-supervised pretraining models for epileptic seizure detection from eeg data,” 2022.
- [41] D. Cai, J. Chen, Y. Yang, T. Liu, and Y. Li, “Mbrain: A multi-channel self-supervised learning framework for brain signals,” 2023.
- [42] R. Cherian and E. G. Kanaga, “Theoretical and methodological analysis of eeg based seizure detection and prediction: An exhaustive review,” *Journal of Neuroscience Methods*, vol. 369, p. 109483, 2022.
- [43] R. Martinek, M. Ladrova, M. Sidikova, R. Jaros, K. Behbehani, R. Kahankova, and A. Kawala-Sterniuk, “Advanced bioelectrical signal processing methods: Past, present and future approach—part ii: Brain signals,” *Sensors*, vol. 21, no. 19, 2021.
- [44] P. LeVan, E. Urrestarazu, and J. Gotman, “A system for automatic artifact removal in ictal scalp EEG based on independent component analysis and Bayesian classification,” *Clinical neurophysiology*, vol. 117, pp. 912–927, 4 2006.
- [45] H. Nolan, R. Whelan, and R. B. Reilly, “FASTER: Fully Automated Statistical Thresholding for EEG artifact Rejection,” *Journal of neuroscience methods*, vol. 192, pp. 152–162, 9 2010.
- [46] I. Winkler, S. Haufe, and M. Tangermann, “Automatic Classification of artifactual ICA-Components for artifact removal in EEG signals,” *Behavioral and brain functions*, vol. 7, p. 30, 1 2011.
- [47] A. Mognon, J. Jovicich, L. Bruzzone, and M. Buiatti, “ADJUST: An automatic EEG artifact detector based on the joint use of spatial and temporal features,” *Psychophysiology*, vol. 48, pp. 229–240, 1 2011.
- [48] L. Frølich, T. Andersen, and M. Mørup, “Classification of independent components of EEG into multiple artifact classes,” *Psychophysiology*, vol. 52, pp. 32–45, 7 2014.
- [49] G. Tamburro, P. Fiedler, D. B. Stone, J. Haueisen, and S. Comani, “A new ICA-based fingerprint method for the automatic removal of physiological artifacts from EEG recordings,” *PeerJ*, vol. 6, p. e4380, 2 2018.

- [50] P. Croce, F. Zappasodi, L. Marzetti, A. Merla, V. Pizzella, and A. M. Chiarelli, “Deep convolutional neural networks for feature-less automatic classification of independent components in multi-channel electrophysiological brain recordings,” 2019.
- [51] L. Pion-Tonachini, K. Kreutz-Delgado, and S. Makeig, “ICLabel: An automated electroencephalographic independent component classifier, dataset, and website,” *NeuroImage*, vol. 198, pp. 181–197, 9 2019.
- [52] S. S. Lee, K. Lee, and G. Kang, “Eeg artifact removal by bayesian deep learning and ica,” 2020.
- [53] F. Lopes, A. Leal, J. Medeiros, M. F. Pinto, A. Dourado, M. Dümpelmann, and C. Teixeira, “Ensemble deep neural network for automatic classification of eeg independent components,” *IEEE Transactions on Neural Systems and Rehabilitation Engineering*, vol. 30, pp. 559–568, 2022.
- [54] F. Lopes, A. Leal, J. Medeiros, M. F. Pinto, A. Dourado, M. Dümpelmann, and C. Teixeira, “EPIC: Annotated epileptic EEG independent components for artifact reduction,” *Scientific data*, vol. 9, 8 2022.
- [55] J. Klatt, H. Feldwisch-Drentrup, M. Ihle, V. Navarro, M. Neufang, C. Teixeira, C. Adam, M. Valderrama, C. Alvarado-Rojas, A. Witon, M. L. Van Quyen, F. Sales, A. Dourado, J. Timmer, A. Schulze-Bonhage, and B. Schelter, “The EPILEPSIAE database: An extensive electroencephalography database of epilepsy patients,” *Epilepsia*, vol. 53, pp. 1669–1676, 6 2012.
- [56] N. J. Stevenson, K. Tapani, L. Lauronen, and S. Vanhatalo, “A dataset of neonatal eeg recordings with seizure annotations,” *Scientific data*, vol. 6, no. 1, pp. 1–8, 2019.
- [57] H. Tekgul, B. F. Bourgeois, K. Gauvreau, and A. M. R. Bergin, “Electroencephalography in neonatal seizures: comparison of a reduced and a full 10/20 montage.,” *Pediatric neurology*, vol. 32 3, pp. 155–61, 2005.
- [58] A. Krizhevsky, I. Sutskever, and G. E. Hinton, “Imagenet classification with deep convolutional neural networks,” in *Advances in Neural Information Processing Systems* (F. Pereira, C. Burges, L. Bottou, and K. Weinberger, eds.), vol. 25, Curran Associates, Inc., 2012.
- [59] C. Feichtenhofer, H. Fan, J. Malik, and K. He, “Slowfast networks for video recognition,” in *Proceedings of the IEEE/CVF International Conference on Computer Vision (ICCV)*, October 2019.
- [60] J. Gehring, M. Auli, D. Grangier, D. Yarats, and Y. N. Dauphin, “Convolutional sequence to sequence learning,” in *Proceedings of the 34th International Conference on Machine Learning* (D. Precup and Y. W. Teh, eds.), vol. 70 of *Proceedings of Machine Learning Research*, pp. 1243–1252, PMLR, 06–11 Aug 2017.
- [61] O. Abdel-Hamid, A.-r. Mohamed, H. Jiang, L. Deng, G. Penn, and D. Yu, “Convolutional neural networks for speech recognition,” *IEEE/ACM Transactions on Audio, Speech, and Language Processing*, vol. 22, no. 10, pp. 1533–1545, 2014.

- [62] K. He, X. Zhang, S. Ren, and J. Sun, “Deep residual learning for image recognition,” in *2016 IEEE Conference on Computer Vision and Pattern Recognition (CVPR)*, pp. 770–778, 2016.
- [63] S. Ioffe and C. Szegedy, “Batch normalization: Accelerating deep network training by reducing internal covariate shift,” in *Proceedings of the 32nd International Conference on Machine Learning* (F. Bach and D. Blei, eds.), vol. 37 of *Proceedings of Machine Learning Research*, (Lille, France), pp. 448–456, PMLR, 07–09 Jul 2015.
- [64] P. Veličković, G. Cucurull, A. Casanova, A. Romero, P. Liò, and Y. Bengio, “Graph Attention Networks,” *International Conference on Learning Representations*, 2018.
- [65] A. Vaswani, N. Shazeer, N. Parmar, J. Uszkoreit, L. Jones, A. N. Gomez, L. u. Kaiser, and I. Polosukhin, “Attention is all you need,” in *Advances in Neural Information Processing Systems* (I. Guyon, U. V. Luxburg, S. Bengio, H. Wallach, R. Fergus, S. Vishwanathan, and R. Garnett, eds.), vol. 30, Curran Associates, Inc., 2017.
- [66] T.-W. Lee, M. Girolami, and T. J. Sejnowski, “Independent component analysis using an extended infomax algorithm for mixed subgaussian and supergaussian sources,” *Neural computation*, vol. 11, pp. 417–441, 1999.
- [67] T.-P. Jung, S. Makeig, M. Westerfield, J. Townsend, E. Courchesne, and T. Sejnowski, “Analysis and visualization of single-trial event-related potentials,” *Human Brain Mapping*, vol. 14, pp. 166 – 185, 11 2001.
- [68] A. Delorme and S. Makeig, “Eeglab: an open source toolbox for analysis of single-trial eeg dynamics including independent component analysis,” *Journal of neuroscience methods*, vol. 134, no. 1, pp. 9–21, 2004.
- [69] K. Raeisi, M. Khazaei, P. Croce, G. Tamburro, S. Comani, and F. Zappasodi, “A graph convolutional neural network for the automated detection of seizures in the neonatal eeg,” *Computer Methods and Programs in Biomedicine*, vol. 222, p. 106950, 2022.

Appendix A

PCB and Schematics

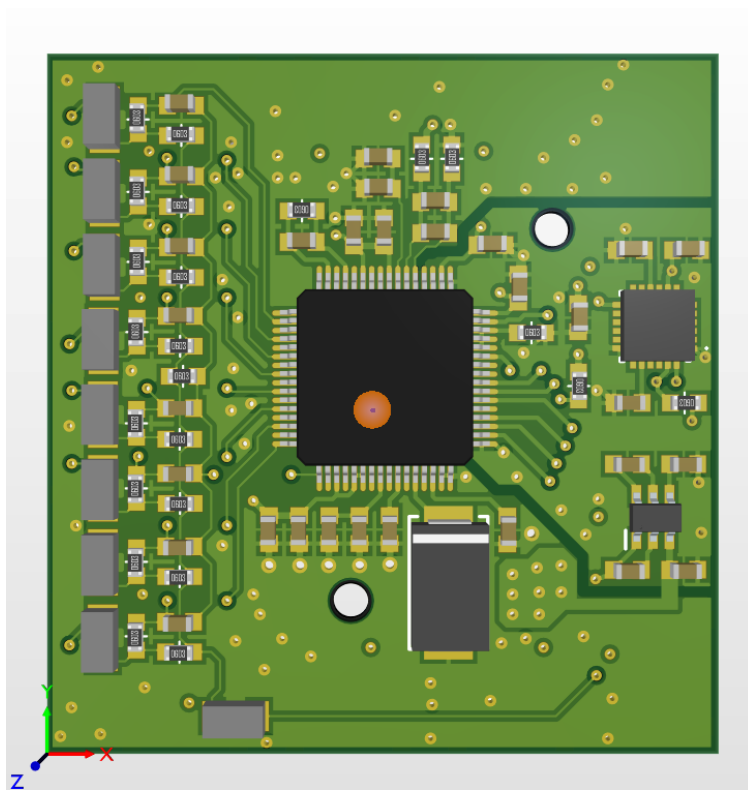


Figure A.1: AFE - 3D view - bottom

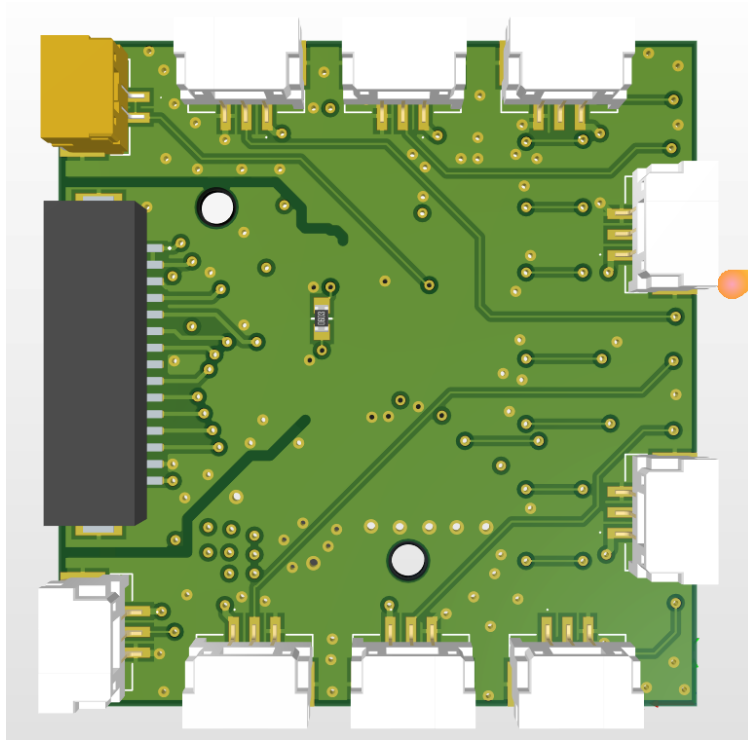


Figure A.2: AFE - 3D view - top

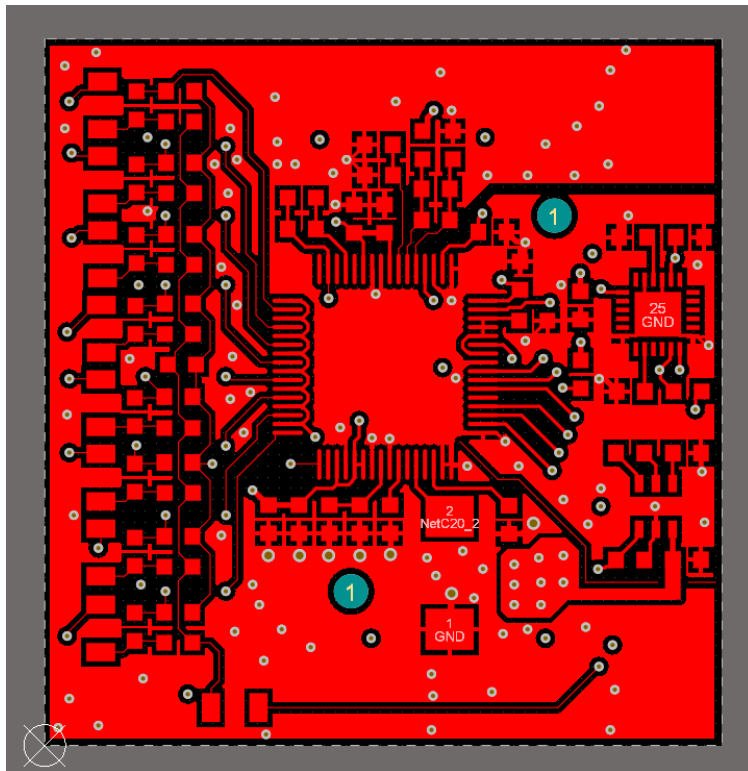


Figure A.3: AFE top layer

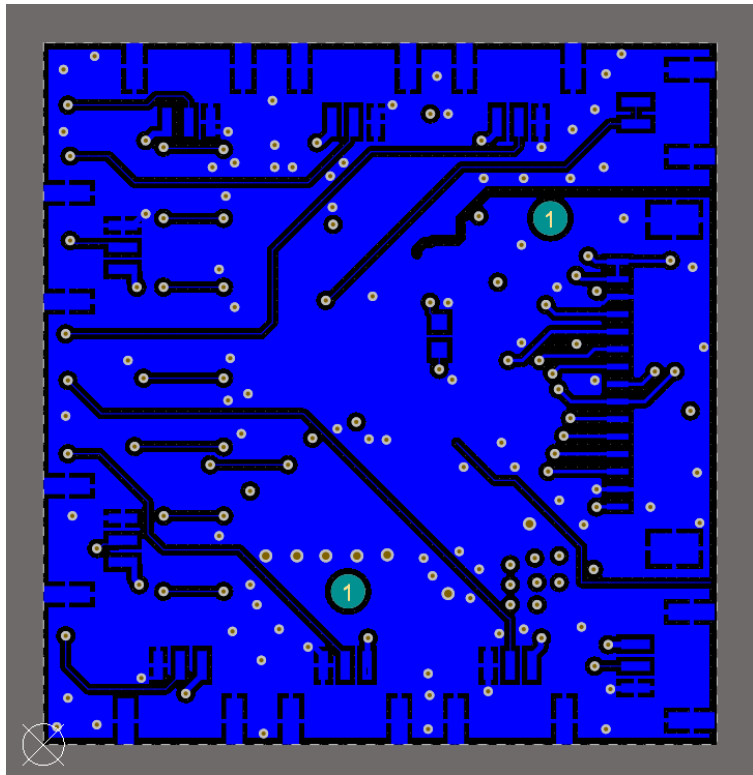


Figure A.4: AFE bottom layer

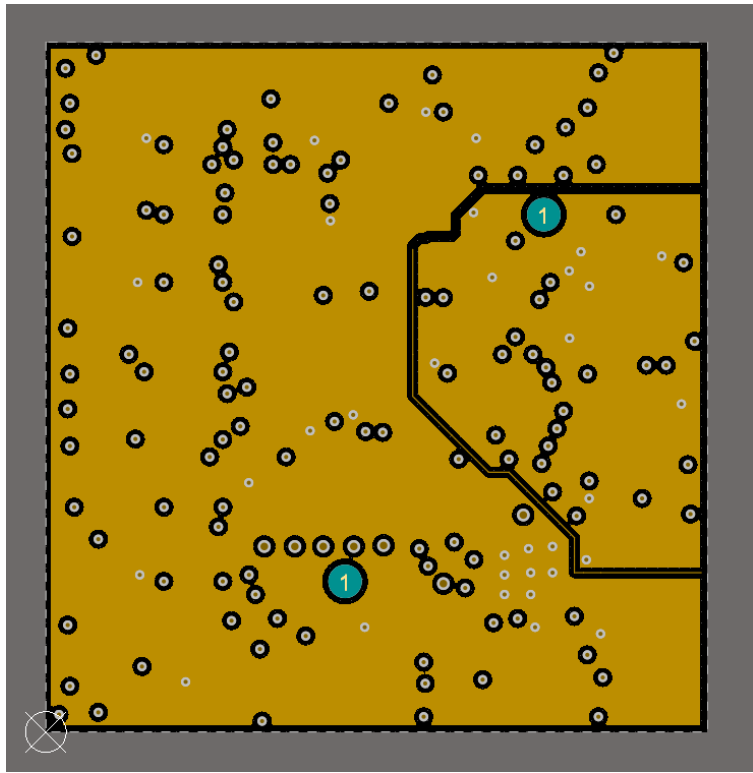


Figure A.5: AFE power layer

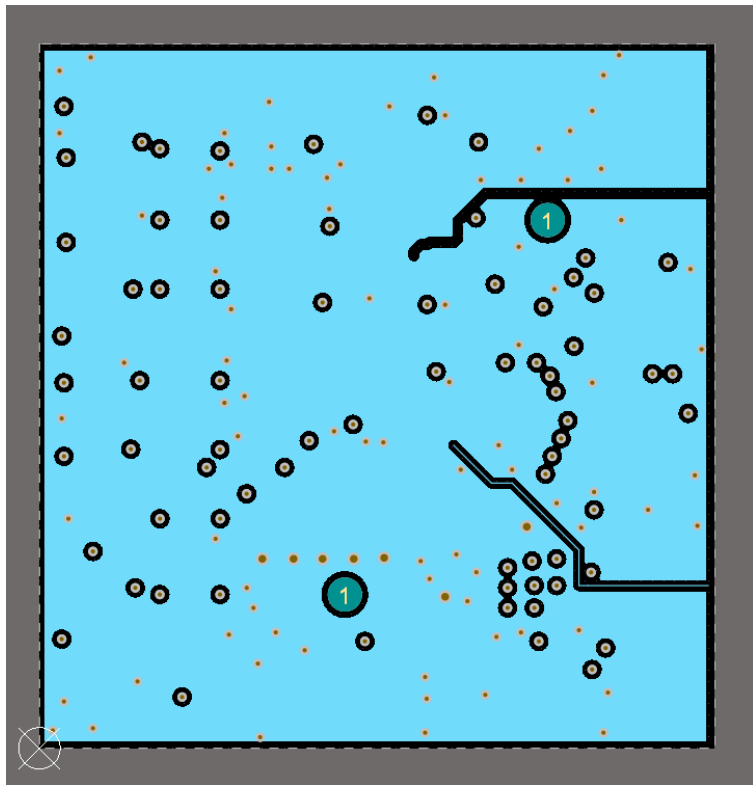


Figure A.6: AFE ground layer

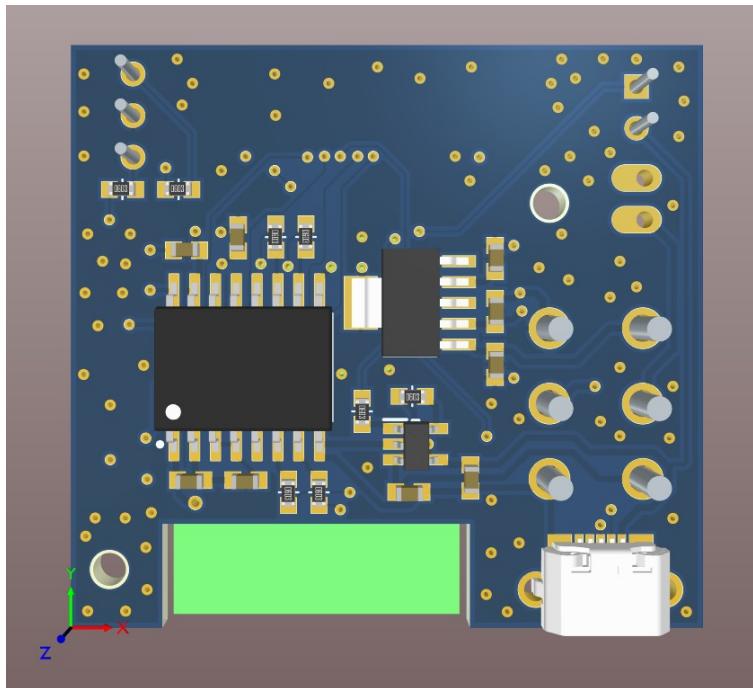


Figure A.7: MCU - 3D view - bottom

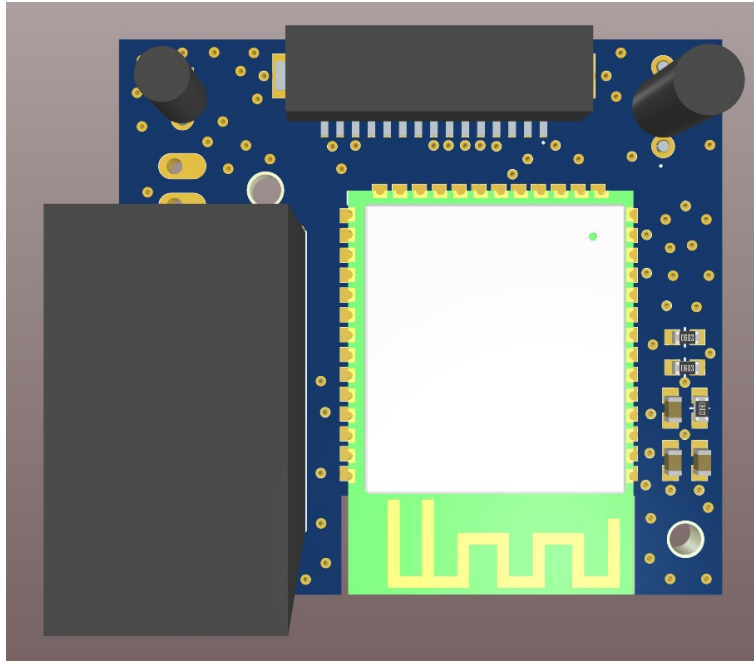


Figure A.8: MCU - 3D view - top

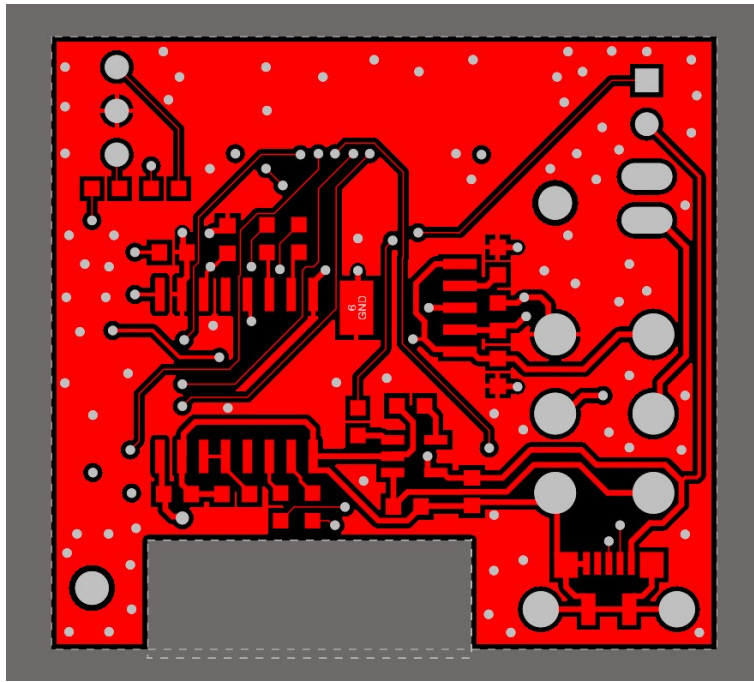


Figure A.9: MCU top layer

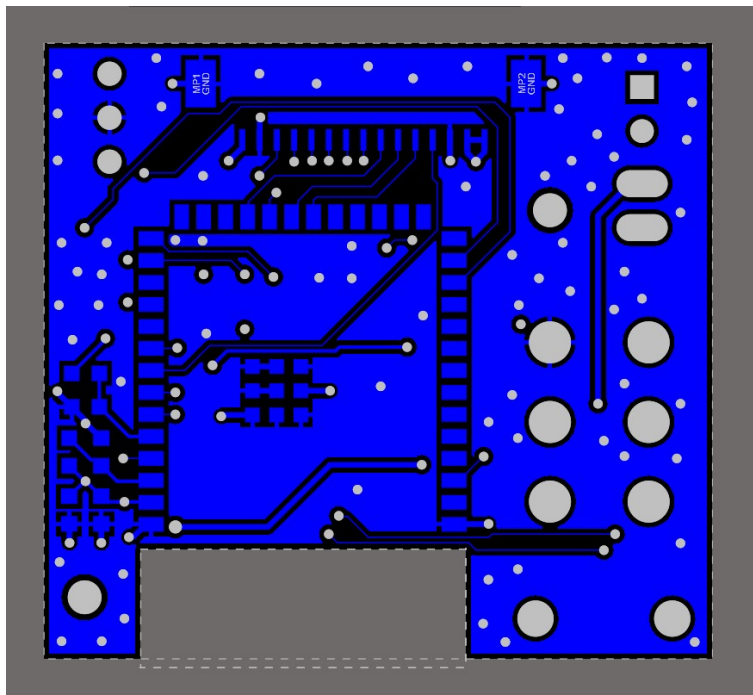


Figure A.10: MCU bottom layer

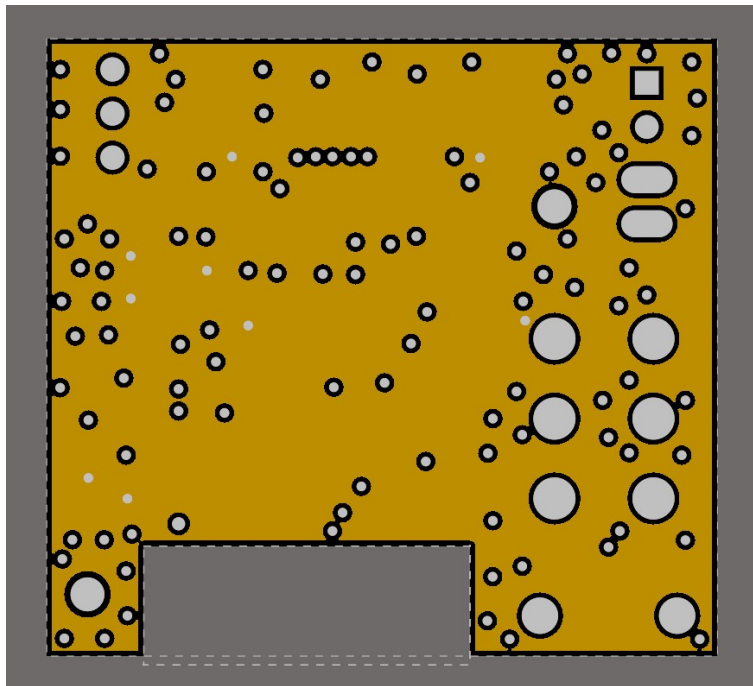


Figure A.11: MCU power layer

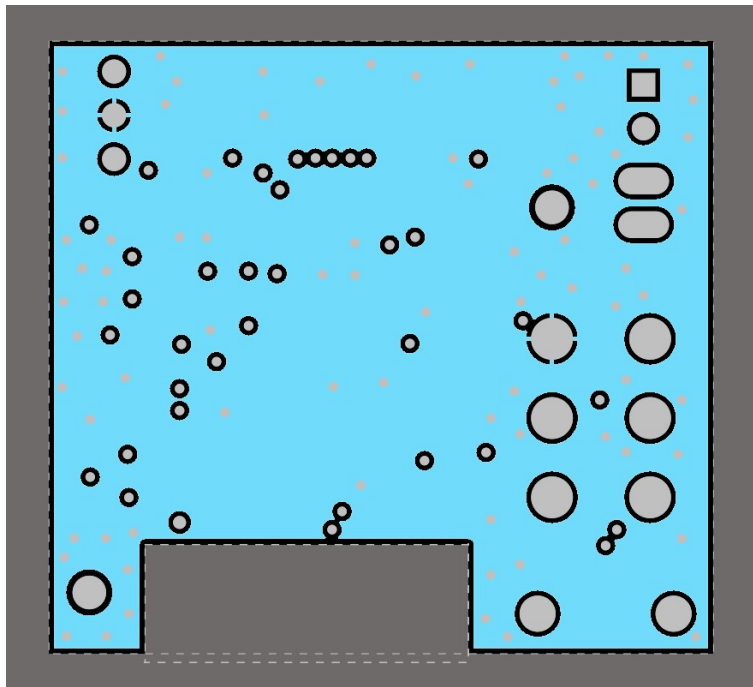


Figure A.12: MCU ground layer

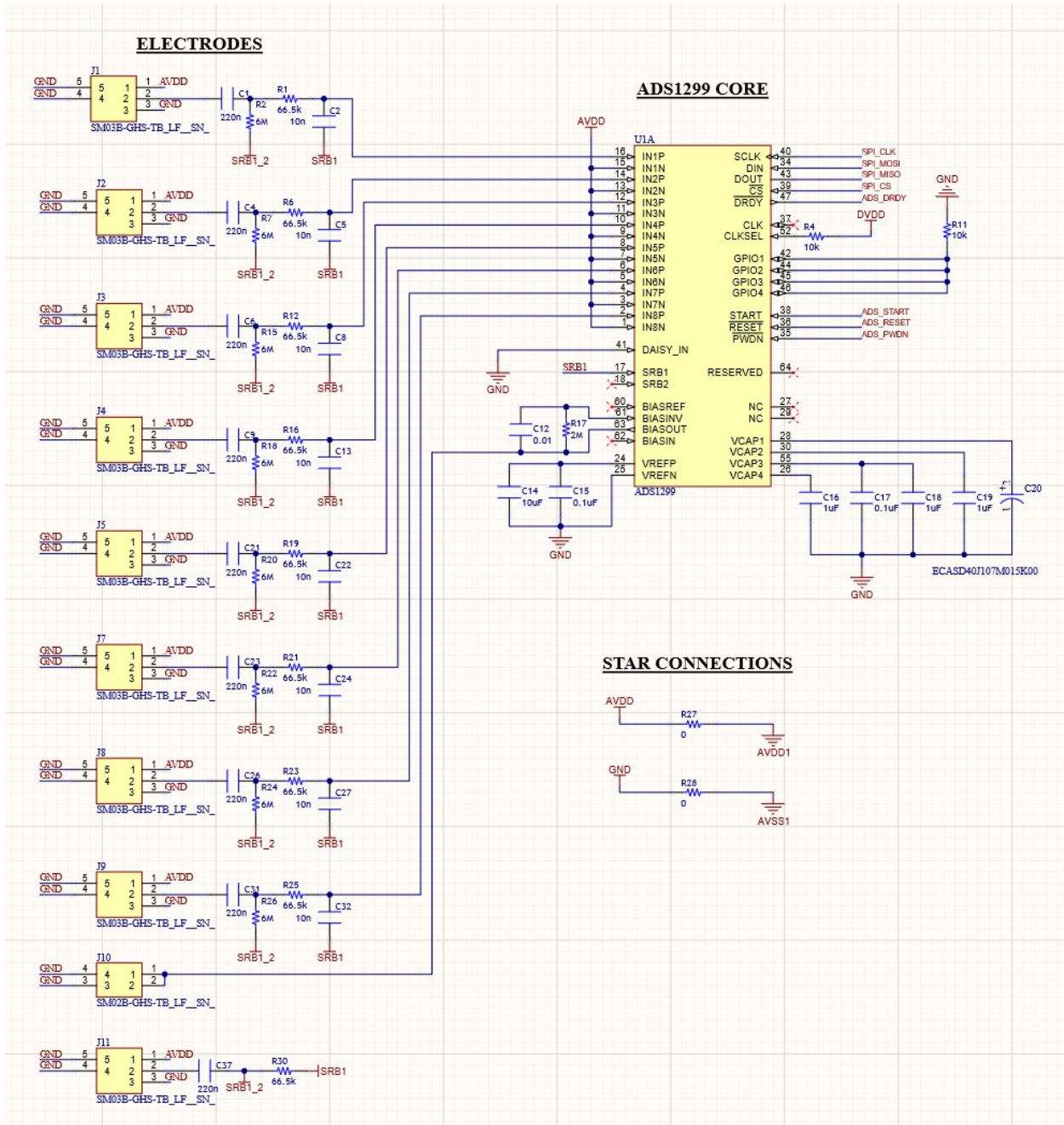


Figure A.13: ADS1299 circuitry

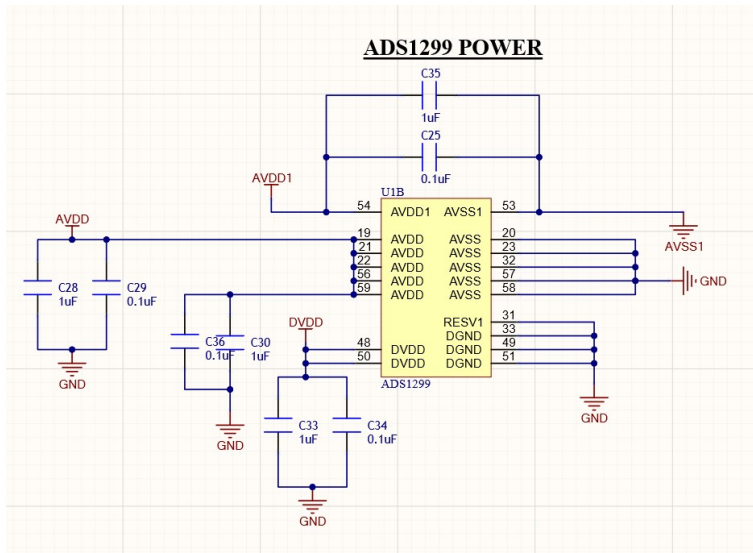


Figure A.14: Power for ADS1299

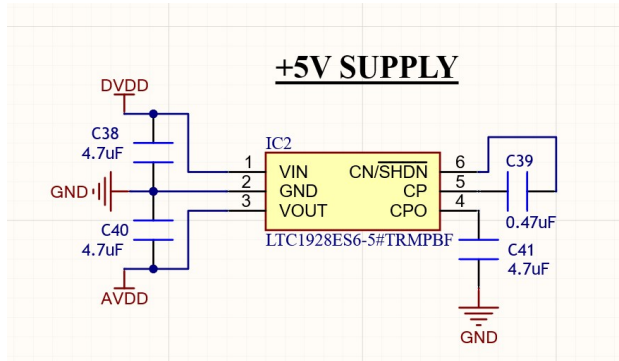


Figure A.15: 5V supply for ADS1299

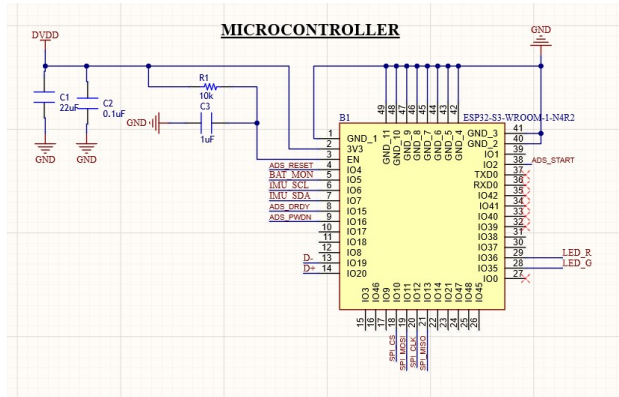


Figure A.16: ESP32 circuitry

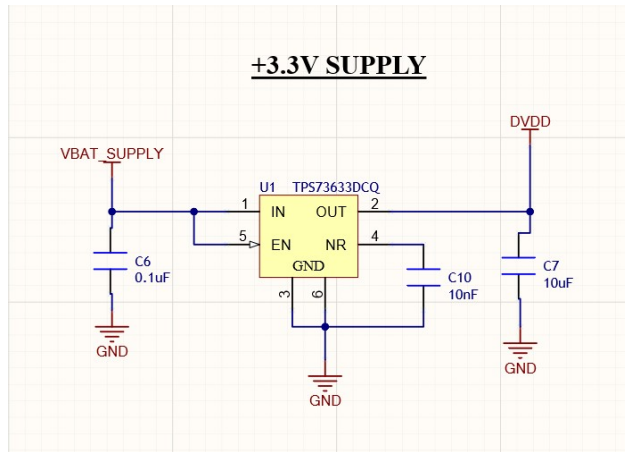


Figure A.17: 3.3V supply for ESP32

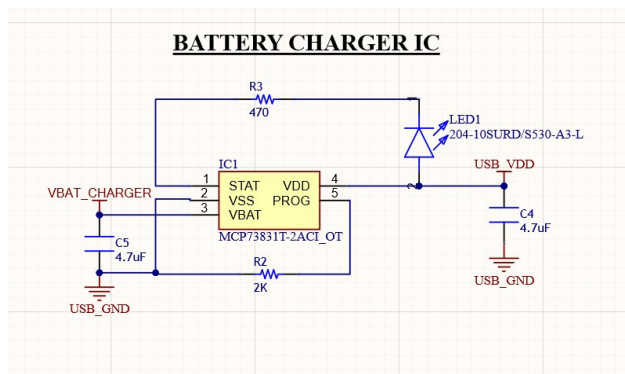


Figure A.18: Battery charging circuit

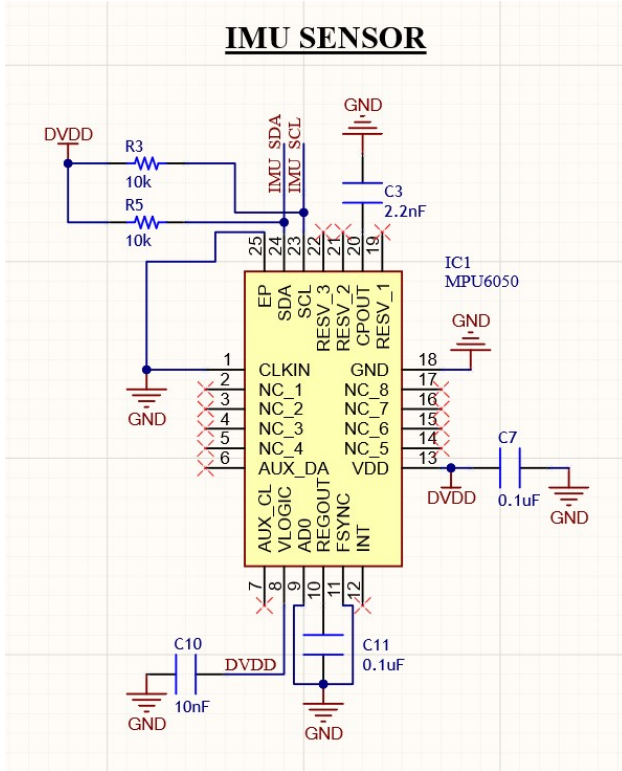


Figure A.19: IMU circuitry

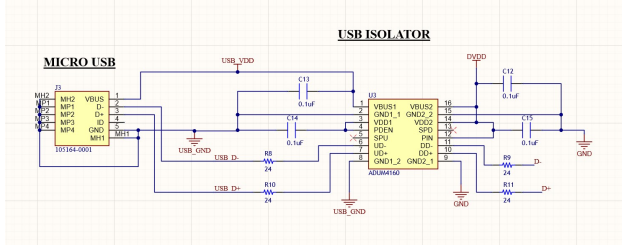


Figure A.20: USB isolator

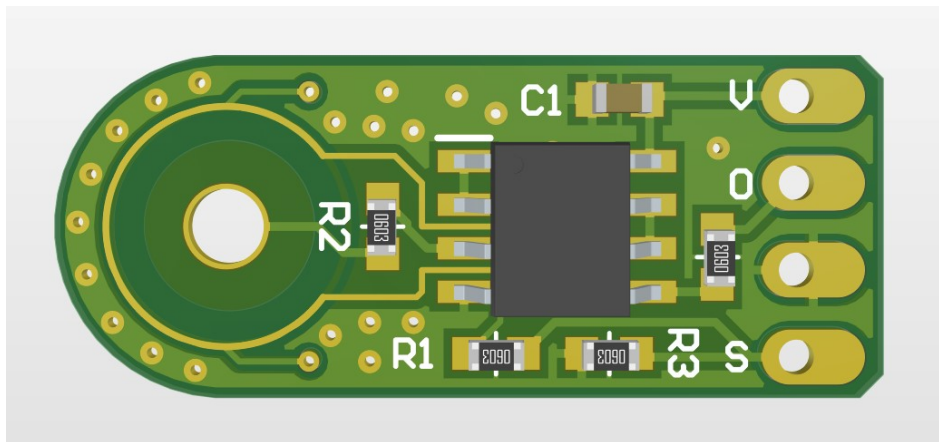


Figure A.21: Active electrode - 3D view - top

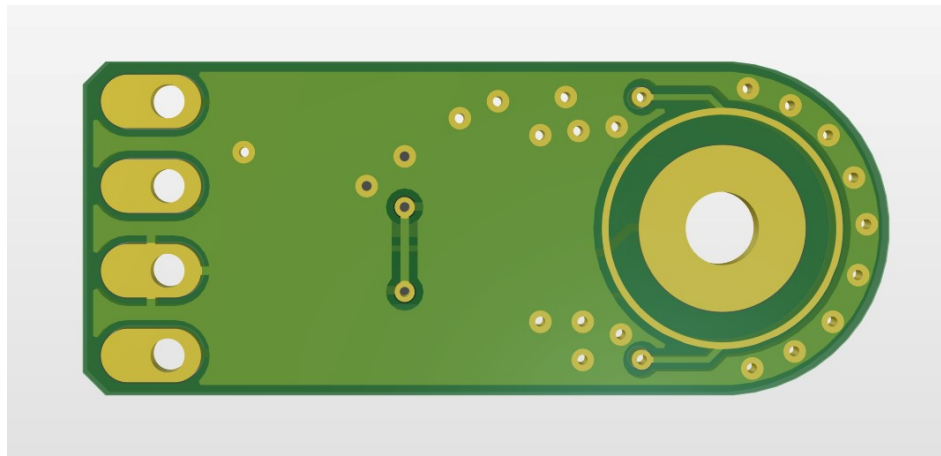


Figure A.22: Active electrode - 3D view - bottom

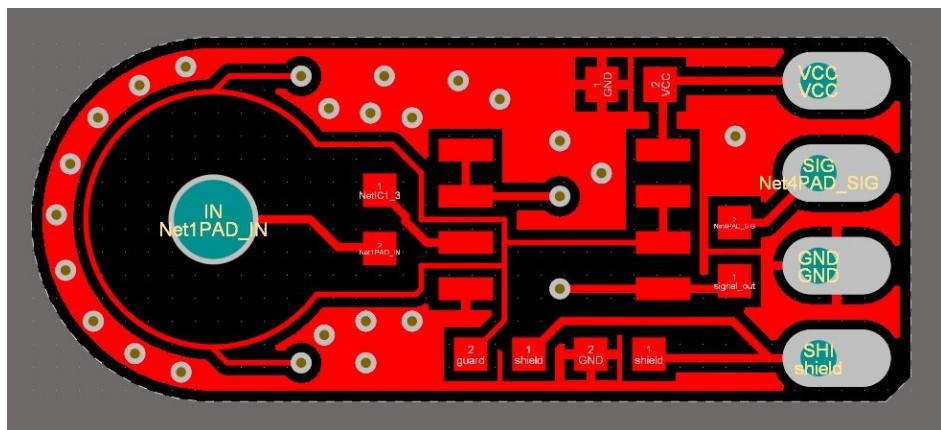


Figure A.23: Active electrode top layer

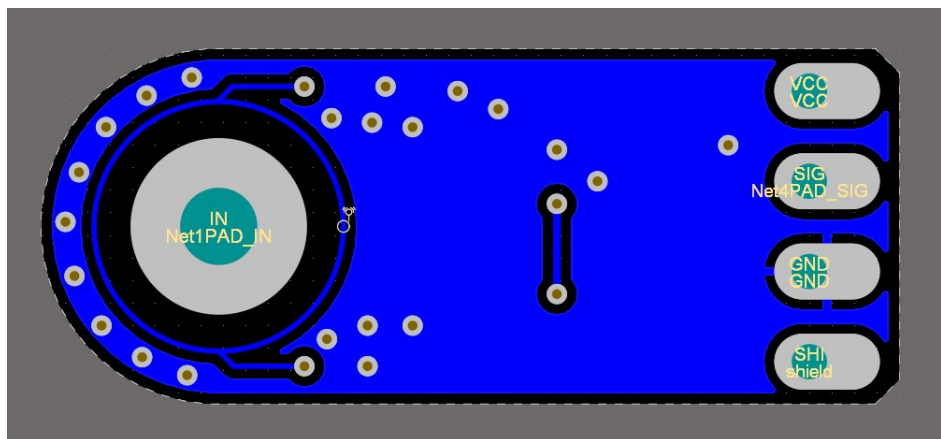


Figure A.24: Active electrode bottom layer

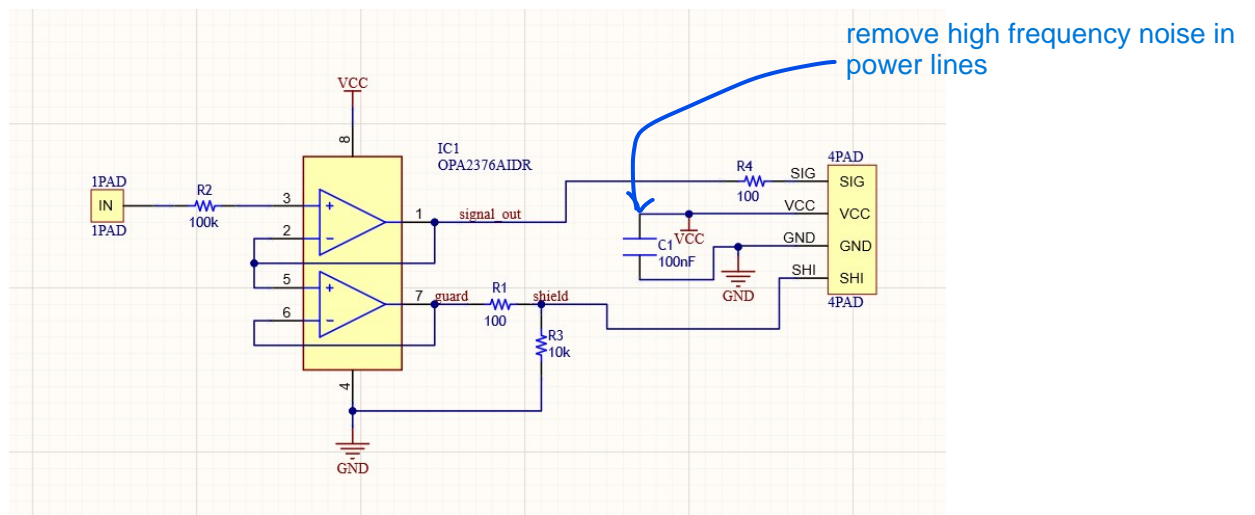


Figure A.25: Active electrode schematics

Appendix B

Information Sheet

Information Sheet

This information sheet is intended for the participants and/or their parents who volunteer from Lady Ridgeway Hospital. The research study is conducted by four biomedical engineering undergraduates from University of Moratuwa. The following are the main personnel involved:

Project: Assess the performance of an AI-Powered User-Friendly Neonatal Seizure Detection Device

Principal Investigator: Dr. Chamira Edussooriya (Senior Lecturer, Dept. of Electronic and Telecommunication Engineering, Faculty of Engineering, University of Moratuwa)

Co-Investigators:

- Dr. Anjula De Silva (Senior Lecturer, Dept. of Electronic and Telecommunication Engineering, Faculty of Engineering, University of Moratuwa)
- Prof. Jithangi Wanigasinghe (Professor in Paediatric Neurology, Faculty of Medicine, University of Colombo, Sri Lanka)
- Dr. Janaka Senarathna (Instructor in Radiology, Johns Hopkins University School of Medicine)
- Kithmin Wickremasinghe (Graduate Research Assistant, University of British Columbia)
- Nima Wickramasinghe (Undergraduate, University of Moratuwa)
- Kavindu Weerasinghe (Undergraduate, University of Moratuwa)
- Dinuka Sandun (Undergraduate, University of Moratuwa)
- Akila Abeyratne (Undergraduate, University of Moratuwa)

1.1 Introduction

This study aims to create an affordable, user-friendly neonatal seizure detection device using EEG and AI technology. We have two main goals: designing EEG signal acquisition hardware and developing an interpretable seizure detection model. This document contains all the details about the research and data collection procedure. Please read it carefully, consult with others if needed, and feel free to ask any questions. Even if you have questions later, feel free to contact the investigators through the contact details provided

1.2 The research study

Neonatal seizures, occurring in infants within the first four weeks after birth, pose a risk, especially for preterm infants. Among preterm infants, this occurs on average in 95 out of every 1000 live births, while in normal infants, the occurrence is 3 out of every 1000 live births. Moreover, one-third of the infants who survive these seizures go on to develop epilepsy later in life. The current diagnosis using continuous EEG is challenging due to resource constraints and practical issues. Our goal is to create an affordable and user-friendly AI-based device for neonatal seizure detection, involving the development of an EEG data acquisition device and an interpretable seizure detection model.

1.3 Type of Research Intervention

Your child will be involved in a completely non-invasive procedure where the following measurement will be acquired.

- EEG signal from the scalp

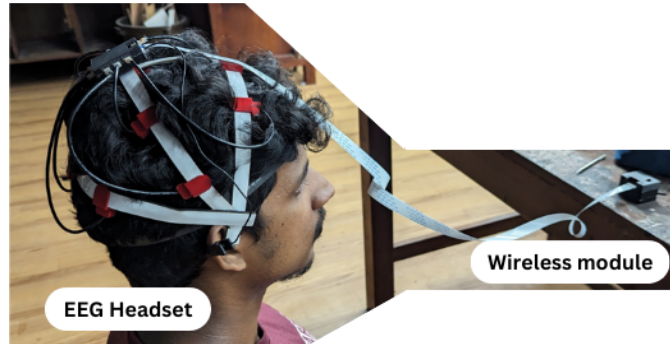


Figure 1: Setup used to capture EEG data

The 9 dry electrodes corresponding to the scalp EEG are attached to a custom-built headwear that covers the most essential parts of the head. When placing the electrodes, gel won't be applied, unlike in the conventional method. All the measurements will be acquired while your child is in a comfortable position same as during the routine checkup during hyperventilation. The signals acquired from the subject will be used to evaluate the system developed for automatic seizure detection.

1.4 Participant selection

We include individuals who are in the age range 6- 16 years experiencing absence seizures requiring regular hyperventilation checkups.

1.5 Voluntary Participation

Your child's participation in this study is voluntary. Your child is free not to participate at all or to withdraw from the study at any time despite consenting to take part earlier. There will be no loss of medical care or any other available treatment for your child's illness or condition to which your child is otherwise entitled. If your child decides not to participate or withdraw from the study, your child may do so at any time.

1.6 Procedure

On the day of the study, you will be explained about the informed consent prior to the procedure.

- Following that, the custom-designed scalp-EEG recording system will be placed on the patient's head.
- Both comfortability and stable contact of the electrode placements will be confirmed.
- Following the confirmation, your child is instructed to start taking deep, rapid breaths, usually through the mouth. The aim is to achieve a rate of about 20 breaths per minute.
- During this process of hyperventilation, the healthcare provider or a trained professional closely monitors the individual for any changes in behavior, signs of discomfort, or the onset of seizures as in the usual procedure, and at the same time, the custom-made EEG system detects if a seizure occurs with the signal obtained.
- The duration of hyperventilation typically lasts for around three to five minutes.
- After the hyperventilation period, the individual is given time to recover and return to their normal breathing pattern. This helps to restore the balance of oxygen and carbon dioxide in the blood. The EEG headset will be removed.
- The attached questionnaire regarding the experience (level of comfort, feedback etc.) will be given before finalizing the procedure.

1.7 Duration

A duration of 10 minutes will be taken for the patient's rest after the initial hyperventilation. The time required for the study is 10 minutes. The patient is instructed to start taking deep, rapid breaths, usually through the mouth, for a duration of 3-5 minutes. After the hyperventilation period, the EEG recording is carried on for another 5 minutes. After the hyperventilation period, the EEG recording is carried out for another 5 minutes during which the individual is given time to recover and return to their normal breathing pattern,. After that, the EEG headset will be removed. After the individual is relaxed he/she, together with their parents, will be asked to fill out the questionnaire, which will take up to 4 minutes. Adding up, the total time will take up to 29 minutes.

1.8 Side Effects

There are no side effects from the acquisition system, but the use of dry electrodes while wearing the EEG cap may cause slight discomfort or skin irritation and, in that case, let the investigators know. Since the data collection process is completely non-invasive, the patient can immediately recover after the data collection process.

1.9 Risks, hazards, and discomforts

Below are the identified risks and the methods to mitigate these risks:

Comfort while wearing EEG headcap: Dry electrodes can sometimes cause mild discomfort, such as itching or redness caused by tight fit. If any of the applied material causes discomfort or irritation to the participant, the experiment will be immediately terminated.

Allergies: The participants could be allergic to the material used in the EEG headcap(Flexible Plastic, velcro, Ag/AgCl electrodes). The participants will be questioned about any allergies to these materials and will be excluded. Even after excluding, if there are any signs of allergies during the experiment, the procedure will be immediately terminated.

Negative effects of hyperventilation: Hyperventilation can cause symptoms such as dizziness, lightheadedness, and shortness of breath. In rare cases, it can also lead to more serious complications, such as fainting or seizures. The participant will be asked whether any such complication has occurred before. If yes, the decision of whether the experiment will be done or not will depend on the opinion of the trained clinician. If any symptom other than what is expected during an absence seizure is observed, the experiment will be stopped, and necessary remedial actions will be taken by the trained clinician.

Any required treatment for the identified risks will be pre-tested and prepared in case of an emergency.

1.10 Potential Benefits

We believe that this study is an important step in the development of a new and innovative way to detect and manage neonatal seizures. We hope that the results of this study will pave the way for further research and development and that this device will ultimately be used to improve the lives of children with this condition.

There are several potential benefits to the participant and for the wider community by participating in this study:

- Helping to develop a low-cost AI-powered device to automatically detect seizures with a future application to detect neonatal seizures
- Improve the diagnosis and monitoring of epilepsy
- Contributing to scientific knowledge

1.11 Reimbursements

Your child will not be paid any sum of money for participating in this study.

1.12 Confidentiality

Your child's identity will be strictly confidential and will not be shared or reported in any format whatsoever. Your child's data will be referred only by a unique code not attached to your child's name.

1.13 Sharing the Results

Your child's identity will never be shared. At the end of the research, we will publish results (Research theses, conferences, and scientific journals) ensuring that the participant's details are anonymized. General information regarding this research program and the conditions and settings could be used to promote or report the university's research efforts through normal media or government reporting channels, but no private data will be used in such activities. Your child can get the results of the study at your child's request.

1.14 Right to Refuse or Withdraw

You/ your child does not have to take part in this research study if you/ your child does not wish to do so. You/your child may also withdraw at any time your child chooses to, even while collecting data (with no penalty or effect on medical care or loss of benefits). Please notify the investigator as soon as you/your child decides to withdraw your child's consent. Please note that if your child withdraws during the recording, it may take up to 2 minutes to remove electrodes before your child can leave the recording room.

1.15 Clarifications

If you have any questions about any of the tests/procedures or information, please feel free to ask any investigator at any time before, while, and after the study has started. You may also contact investigators for further clarifications through the following contact details:

Dr. Chamira Edussooriya (071-1656562)

Prof. Jithangi Wanigasinghe (077-7313914)